AD-A190 822 AC IMPEDANCE ANALYSIS OF CORROSION FATIGUE IN NAVAL AIRCRAFT ALLOYS..(U) ROCKWELL INTERNATIONAL THOUSAND OAKS CA SCIENCE CENTER M KENDIG ET AL. MAY 87 1/1

UNCLASSIFIED SC5436.2FR NADC-87103-60 N62269-85-R-0248 F/G 11/6.1 NL

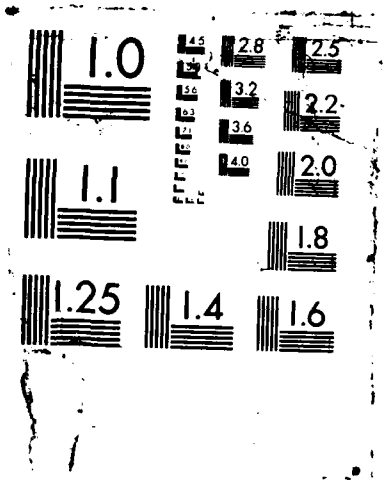
1.0
1.1
1.25
1.4
1.6
1.8
2.0
2.2
2.5
2.8
3.2
3.6
4.0

REPORT NO. NADC-87183-60

DTIC FILE COPY

AD-A190 822

AC IMPEDANCE ANALYSIS OF CORROSION FATIGUE IN NAVAL AIRCRAFT ALLOYS

M. Kendig and F. Mansfield
Rockwell International
Science Center
Thousand Oaks, CA 91360

MAY 1987

FINAL REPORT
Contract No. N62269-85-R-0248

Approved for Public Release:
Distribution Unlimited

Prepared for
NAVAL AIR DEVELOPMENT CENTER
Department of the Navy
Warminister, PA 18974-5000

UNCLASSIFIED
SECURITY CLASSIFICATION OF THIS PAGE A190222

REPORT DOCUMENTATION PAGE

1a. REPORT SECURITY CLASSIFICATION UNCLASSIFIED	1b RESTRICTIVE MARKINGS
2a. SECURITY CLASSIFICATION AUTHORITY	3 DISTRIBUTION / AVAILABILITY OF REPORT Approved for public release; distribution unlimited.
2b. DECLASSIFICATION / DOWNGRADING SCHEDULE	
4. PERFORMING ORGANIZATION REPORT NUMBER(S) SC5436.2 FR	5 MONITORING ORGANIZATION REPORT NUMBER(S) Report No. NADC-87183-60
6a NAME OF PERFORMING ORGANIZATION ROCKWELL INTERNATIONAL Science Center 6b OFFICE SYMBOL (*If applicable*) N/A	7a. NAME OF MONITORING ORGANIZATION Naval Air Development Center
6c. ADDRESS (*City, State, and ZIP Code*) 1049 Camino Dos Rios Thousands Oaks, CA 91360	7b. ADDRESS (*City, State, and ZIP Code*) Warminster, PA 18974-5000
8a. NAME OF FUNDING / SPONSORING ORGANIZATION Naval Air Development Center 8b OFFICE SYMBOL (*If applicable*) 6062	9. PROCUREMENT INSTRUMENT IDENTIFICATION NUMBER Contract No. N62269-85-85-R-0248
8c. ADDRESS (*City, State, and ZIP Code*) Warminster, PA 18974-5000	10. SOURCE OF FUNDING NUMBERS PROGRAM ELEMENT NO. 61153N; PROJECT NO. R02202; TASK NO WR02202; WORK UNIT ACCESSION NO. AT580

11. TITLE (*Include Security Classification*)
AC IMPEDANCE ANALYSIS OF CORROSION FATIGUE IN NAVAL AIRCRAFT ALLOYS

12. PERSONAL AUTHOR(S)
Kendig, M. and Mansfeld, F.

13a. TYPE OF REPORT	13b TIME COVERED	14. DATE OF REPORT (*Year, Month, Day*)	15 PAGE COUNT
Final Report	FROM 08/10/85 TO 11/30/86	1987, MAY	56

16. SUPPLEMENTARY NOTATION

17 COSATI CODES			18 SUBJECT TERMS (*Continue on reverse if necessary and identify by block number*)
FIELD	GROUP	SUB-GROUP	Corrosion, Fatigue, Steel, Aluminum, AC Impedence, Corrosion Inhibitor, Crack Tip

19 ABSTRACT (*Continue on reverse if necessary and identify by block number*)

The objective of this progam is to develop rapid electrochemical methods for evaluating the susceptibility of Naval aircraft materials to corrosion fatigue (CF). A fatigue admittance method that evaluates the coupling of the modulated stress intensity factor to electrochemical reation kinetics has been developed. In addition, phase sensitive detection of the crack tip displacement allows continuous measurement of the CF rate as a function of time and potential. Application of fatigue admittance analysis to the CF of Al 7075-T73 demonstrates that the crack tip of the material in aerated 0.5 M NaCLis anodic to the nonoccluded surface of the material. Injection of a corrosion inhibitor (DNBM) into the crack tip decreases the extent to the anodic polarization of the crack tip and decress the electrochemical rate of oxidation in hte crack tip by a factor of 100. The role of aqueous and organic phase dichromate, nitrite, borate and molybdate (DNBM) on the CF rate of 4340 steel in 0.5 NaCl has also been evaluated. The organic complex DNBM when injected in the crack tip reduces the crack growth rate by a factor of 10. The aqueous inhibitors at a concentration level of 0.01 M show only small influences on the open CF rate, but

20 DISTRIBUTION / AVAILABILITY OF ABSTRACT ☐ UNCLASSIFIED/UNLIMITED ☒ SAME AS RPT ☐ DTIC USERS	21 ABSTRACT SECURITY CLASSIFICATION UNCLASSIFIED
22a NAME OF RESPONSIBLE INDIVIDUAL Dr Vinod S. Agarwala	22b TELEPHONE (*Include Area Code*) (215) 441-1122 22c OFFICE SYMBOL 6062

DD FORM 1473, 84 MAR 83 APR edition may be used until exhausted
All other editions are obsolete

SECURITY CLASSIFICATION OF THIS PAGE
UNCLASSIFIED GPO: U.S. Government Printing Office: 1985—507-047

0.01 M borate reduces the cathodically aerated CF. The molybdate and dichromate inhibitors at the 0.01 M level appear to show the anodic reaction in the crack tip. The maximum load has a dominating influence on the electrochemical kinetics in the crack tip.

As part of a technology transfer task, electrochemical impedance spectra for 4340 steel pretreated with a mixed inhibitor in an organic solution (DNBM) supplied by NADC were evaluated in serated 0.5 M NaCL Analysis of the spectra demonstrates that the corrosion rate of the steel treated with the inhibitor decreases by about a factor of 100. The inhibition mechanism involves interphase inhibition due to the formation of a three-dimensional film. Electrochemical impedance spectra have also been used to evaluate chemically filmed Al 2024 and 7075 surfaces prepared by NADC. The results demonstrate that a chemical conversion coating on Al 7075 which contains 10% dichromate, molybdate, nitrite and borate solvated in xylene by long chain alkyl ammonium cations increases the corrosion resistance of the Al 7075 by a factor of 1000 over the bare Al 7075 and by a factor of 100 over the conversion coted Al without the inhibitors. It is recommended that this method be further tested for practical use in aerospace structures.

TABLE OF CONTENTS

		Page
1.0	INTRODUCTION	1
2.0	EXPERIMENTAL METHODS	3
2.1	Fatigue Current Measurement	3
2.2	Crack Growth Rate Monitoring	6
2.3	Inhibitor Systems	7
2.4	Experiments Designed to Probe the Role of Inhibiting Species on the Crack Tip Electrochemical Kinetics	8
2.5	Electrochemical Impedance Measurements	9
3.0	RESULTS	10
3.1	Fatigue Admittance of Al 7075-T73	10
3.1.1	Influence of Mechanical and Electrochemical Variables on I_{ac} for Al 7075-T73	10
3.1.2	Dependence of I_{ac} on Potential and the Presence of Inhibitor	13
3.2	Fatigue Admittance for 4340 Steel - Influence of Aqueous Anionic Inhibitors on the Crack Tip Electrochemical Reactions	14
3.3	Evaluation of Corrosion Protection by Inhibitors and Coatings	24
3.3.1	Evaluation of a Mixed Inhibitor for Steel	25
3.3.2	Evaluation of Conversion Coatings for Aluminum 2024	29
3.3.3	Impedance of Conversion-Coated and Inhibitor-Treated Al 7075	31
4.0	SUMMARY, CONCLUSIONS AND RECOMMENDATIONS	40
5.0	REFERENCES	42
6.0	ACKNOWLEDGEMENT	44
	APPENDIX I. - SYMBOLS AND ABBREVIATIONS	45
	APPENDIX II. - STATISTICAL ANALYSIS	47

LIST OF FIGURES

Figure		Page
1	Schematic showing the specimen dimensions and placement of the masking material.	4
2	(a) Schematic of the fatigue admittance test apparatus.	4
	(b) Photograph of the apparatus	5
3	Schematic for the continuous compliance monitoring.	6
4	Calibration curve for crack length vs compliance for 4340 steel (R_c 52). Experimental conditions: R = 0.5, f = 1 Hz, K_{max} = 35 MPa$\sqrt{m}$.	7
5	Time dependence for the fatigue current, I_{ac}, for Al 7075-T73 in 0.5 M NaCl at 4 Hz.	10
6	R-ratio dependence for the fatigue current, I_{ac}, for Al 7075-T73 in 0.5 M NaCl at 4 Hz using constant mean load of 321 MPa$\sqrt{mm}$, or constant maximum amplitude of 427 MPa$\sqrt{mm}$	11
7	I_{ac} as a function of ΔK_{si} for the data from Fig. 6.	12
8	I_{ac} as a function of $\Delta K_{si,max}$ for the data from Fig. 6.	12
9	Potential dependence for I_{ac} and I_{dc} for a fatigue specimen of Al 7075-T73 in 0.5 M NaCl at 4 Hz before and after injection of an isopropanol solution of DNBM inhibitor into the crack.	13
10	Potential dependence for the (a) crack growth rate for 4340 steel in 0.5 M NaCl with and without injection of DNBM inhibitor into the crack tip, (b) I_{ac} and I_{dc} vs potential in 0.5 M NaCl without DNBM, and (c) I_{ac} and I_{dc} vs potential in 0.5 M NaCl with DNBM. The conditions: f = 1 Hz, R-ratio = 0.5 and K_{max} = 34 MPa$\sqrt{mm}$	15
11	$E_o - E_c$ plotted as a function of dA/dN_o for 4340 steel and the conditions of Table 1	22
12	$I_{ac}(E_o)$ plotted as a function of E_o-E_c for 4340 steel and the conditions of Table 1.	22

LIST OF FIGURES (continued)

Figure		Page
13	E_o plotted as a function of dA/dN_c-dA/dN_o, the difference between the CF rate at -900 mV_{SCE} and the corrosion potential, for 4340 steel and the conditions of Table 1.	23
14	$1/R_{xp}$ plotted as a function of E_o-E_c for 4340 steel and the conditions of Table 1.	23
15	$1/R_{xp}$ plotted as a function of dA/dN_c-dA/dN_o, the difference between the CF rate at -900 mV_{SCE} and the corrosion potential, for 4340 steel and the conditions of Table 1.	24
16	Bode plots for rotating and stagnant inhibited steel cylinder electrodes in 0.5 M NaCl after exposure times of 5 and 23 h.	26
17	Nyquist plots for 4340 steel RCE with and without DNBM at different exposure times.	27
18	Equivalent circuit and simulated impedance plots for the blocked surface model.	28
19	Computerized fit of blocked surface model for the results from the 4340 steel RCE with and without DNBM at 5 h	28
20	Bode-plots for Al 2024 with two different conversion coatings during exposure to 0.5 M NaCl, pH = 4.	30
21	Same as Fig. 20 but at neutral pH.	30
22	Bode plots for Al 7075 in aerated 0.5 M NaCl after 1, 23 and 46 h.	32
23	Bode plots for chromate conversion coated (CCC) Al 7075-T73 in aerated 0.5 M NaCl after 1, 4 and 23 h.	34
24	Bode plots for chromate conversion coated Al 7075 treated with DNBM (CCC-DNBM) in aerated 0.5 M NaCl after 1, 23, 46 and 218 h	35
25	Bode plots for chromate containing molybdate conversion-coated Al 7075 in aerated 0.5 M NaCl between 1 and 242 h. The surface was additionally treated with DNBM after 23 h.	36

LIST OF FIGURES (continued)

Figure		Page
26	Bode plots for chromate containing molybdate conversion-coated and DNBM treated Al 7075 in aerated 0.5 M NaCl between 1 and 339 h.	37
27	Time dependence for R_p, C_p and E_o for the Al 7075 alloys having different surface treatments.	39

LIST OF TABLES

Table		Page
1	Test Conditions for Inhibitor Matrix	8
2	Summary of Fatigue Current Results for DNBM Inhibition into the Crack	14
3	Summary of Results from Test Matrix	17
4	Ratio of Mean Squares	18
5	Regression Analysis	21
6	R_d, R_d* and R_{me} for 4340 Steel RCE With and Without DNBM Corrosion Inhibitor	29

1.0 INTRODUCTION

The overall objective of this program is to develop rapid methods for the evaluation of the susceptibility of aircraft materials to corrosion fatigue (CF) and to transfer the technology to the Naval Air Development Center. Electrochemical transient methods for the rapid evaluation of the susceptibility of Al alloys and steel to CF and electrochemical impedance spectroscopy (EIS) methods have been explored. EIS has been found to be particularly applicable to the evaluation of corrosion inhibition of steel and corrosion protection afforded to Al alloys by conversion coatings in environments where these materials are susceptible to CF. Cyclic electrochemical transients due to cyclic loading of cracked Al 7075 and 4340 steel (R_c = 52) specimens which can be used to evaluate the role of inhibitors at the crack tip have been observed.

CF results from enhanced localized corrosion engendered by localized plastic deformation which leads to the disruption of otherwise protective films.[1,2] Since corrosion is an electrochemical process that depends on the transfer of electrons from oxidation sites on the metal surface to sites where the oxidant, typically oxygen or hydrogen ion, is reduced, a reasonable method of rapidly and directly quantifying the contribution of corrosion to fatigue would involve measuring the coupling of electrochemical currents to stress intensity, ΔK_{si}. Observation of the ac fatigue current, I_{ac}, having the same frequency as the cyclic stress intensity, ΔK, can be used to define a coupling coefficient, $I_{ac}/\Delta K_{si}$ referred to in this report as the "fatigue admittance". Alternatively, if ΔK_{si} remains constant for a given series of tests, it is more convenient to use I_{ac} to define the coupling of the electrochemical processes to the stress intensity. By providing direct evaluation of the electrochemical kinetics for the metal dissolution/oxidation localized at the crack tip, this method constitutes a valuable tool for assessing the behavior of different material/environment combinations. Therefore, the technique of fatigue admittance will be particularly important to the development of materials for Naval aircraft such as high-strength steels and Al alloys exposed to environments of high chloride concentration.[3]

Only recently has serious attention been directed toward the development of techniques applicable for direct observation of the coupling of electrochemical reactions to applied cyclic stress.[3,5-9] Work previously performed in this laboratory initiated the novel approach of using phase-sensitive detection of the small ac signal from a potentio-

stated fatigue specimen containing a growing crack.[4] Phase sensitive detection of the cyclic displacement of the crack growth has also been used to continuously and virtually instantaneously monitor the sample compliance and, hence, crack growth rate in situ, thereby enabling the generation of crack growth rate vs potential curves. These methods have been applied to investigate the CF mechanism of high-strength Al 7075-T73 and the role of inhibitors in reducing the CF of 4340 steel (R_C52).

2.0 EXPERIMENTAL METHODS

2.1 Fatigue Current Measurements

Several methods were considered for optimizing the collection and evaluation of the ac current resulting directly from the applied cyclic stress during CF. Since the ac current (I_{ac}) from the fatigue process is, in general, superimposed on a high dc current and may be many dB below the noise from other sources, such as 60 cycles induced from the line, several methods for enhancing the isolation of I_{ac} were considered. First, the constant-K, fatigue specimen was coated with an insulating masking material (Turco-mask) except for a portion of the surface surrounding the notch, as shown in Fig. 1. This minimized the dc offset due to currents flowing from the bulk of the specimen when a potential was applied. In addition, the current from the potentiostat was input to a low pass, differential amplifier (Tektronix Model 501) shown in Fig. 2. A differential method for eliminating the large dc offset was first attempted by observing the differential current from nearly identical specimens; one was fatigued and the other served as the reference specimen. This approach provided no additional advantage. Line noise was minimized by placing all of the instruments on a line filter.

The amplified and conditioned I_{ac} signal from the differential amplifier was fed into the lock-in amplifier (LIA) that demodulates the signal which was locked to the applied load. All ac noise containing frequency components different from that of the applied level and having random phase are averaged out during the detection process and only I_{ac} remains. The optimum time constant for the LIA output was 4 s. The resulting ac signal from the LIA, which is proportional to I_{ac}, and the average dc signal from the current amplifier, which is proportional to dc polarization current I_{dc}, were recorded on a strip chart recorder. A number of experiments were performed by sweeping the potential about the open-circuit potential at a rate of 0.1 mV/s. At this rate, the system response is sufficiently slow to accommodate the 4 s time constant.

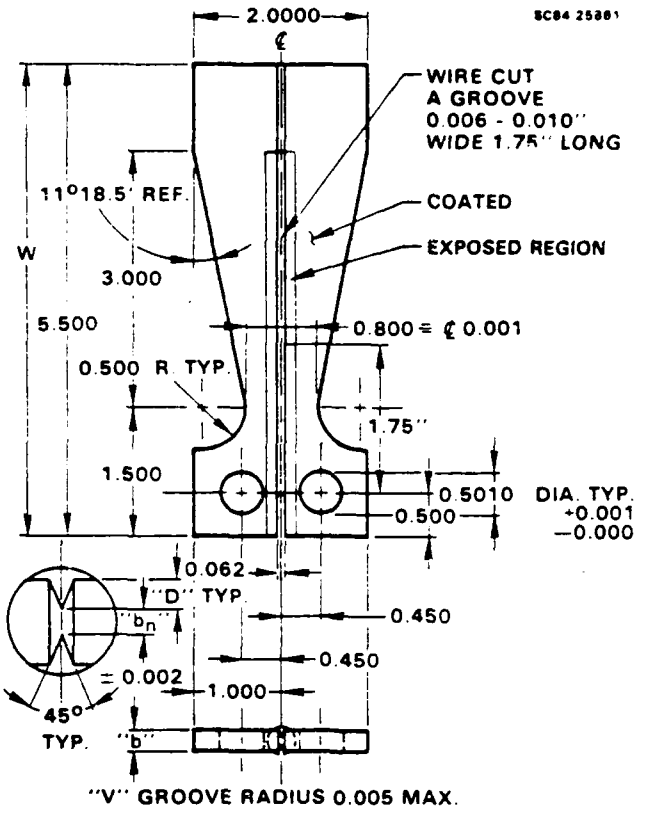

Fig. 1 Schematic showing the specimen dimensions and placement of the masking material.

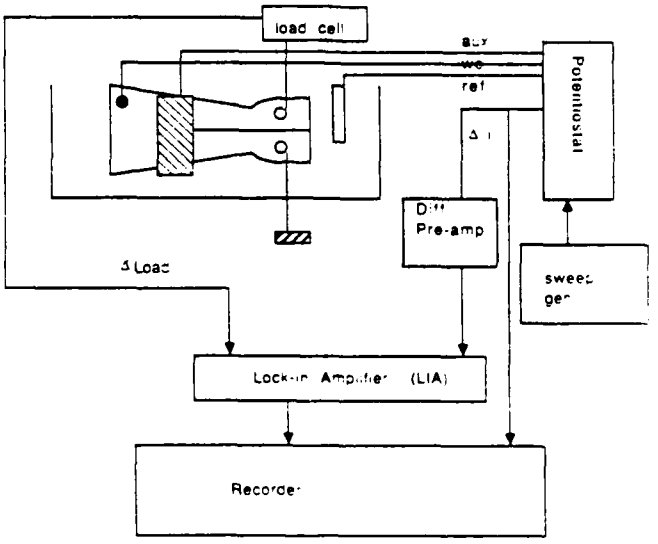

Fig. 2 (a) Schematic of the fatigue admittance test apparatus.

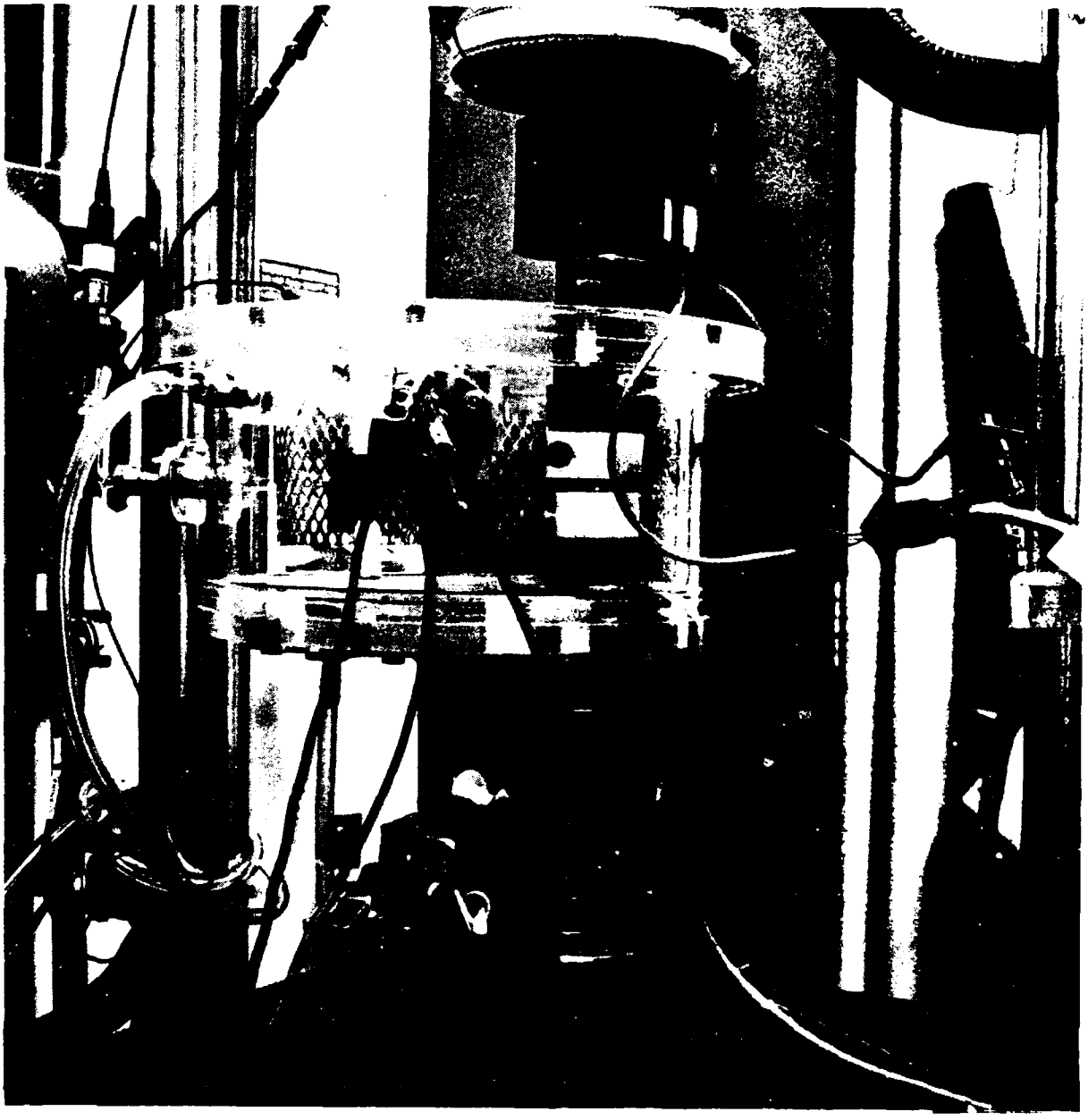

2.2 Crack Growth Rate Monitoring

To monitor the crack growth rate for comparison with the fatigue currents observed for 4340 steel, an extensometer system was designed and constructed. This was necessary since corrosion products formed on the exposed surface of the fatigue specimen precluded direct observation of scribed calibration marks using a long distance microscope. Figure 3 shows a schematic of the extensometer system. The compliance defined as the change in extension/load could be related to the crack length using the calibration curve shown in Fig. 4. This curve was determined from the observed compliance at the end of a test. The crack length was evaluated from a measurement of the corroded portion of the fracture surface determined after destructively overloading the specimen to failure in air following the test. Use of the lock-in amplifier to phase sensitively detect the fluctuating extension allowed continuous measurement of the rate of change in extension at the level of 1Å/s which corresponds roughly to a sensitivity of 0.01 μm/cycle at 1 Hz (Fig. 4). As a result, compliance vs potential could be determined continuously as a function of applied potential.

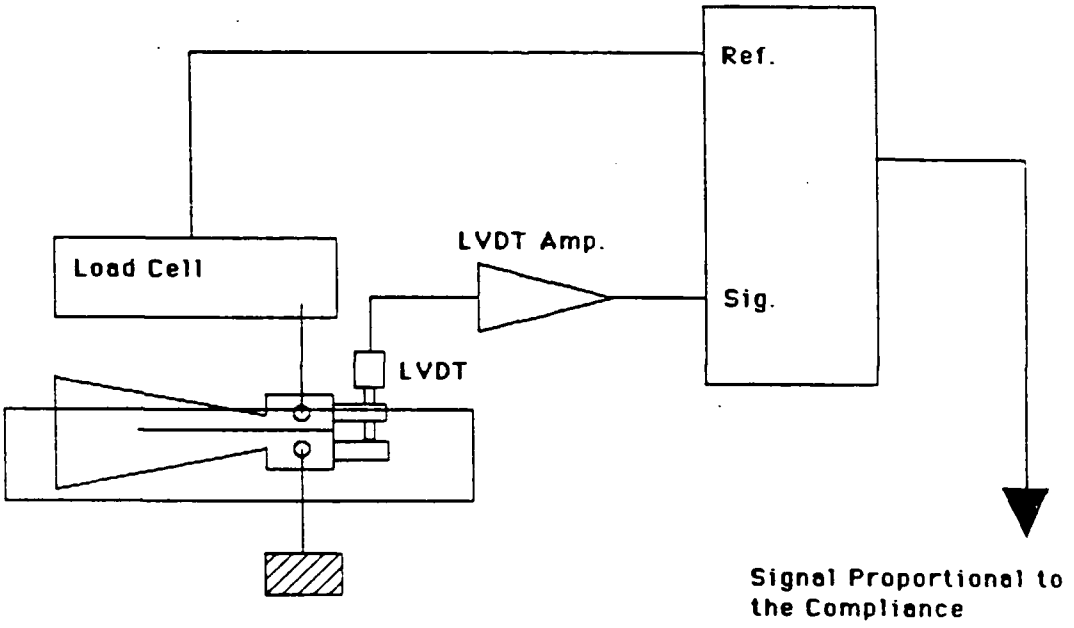

Fig. 3 Schematic for the continuous compliance monitoring.

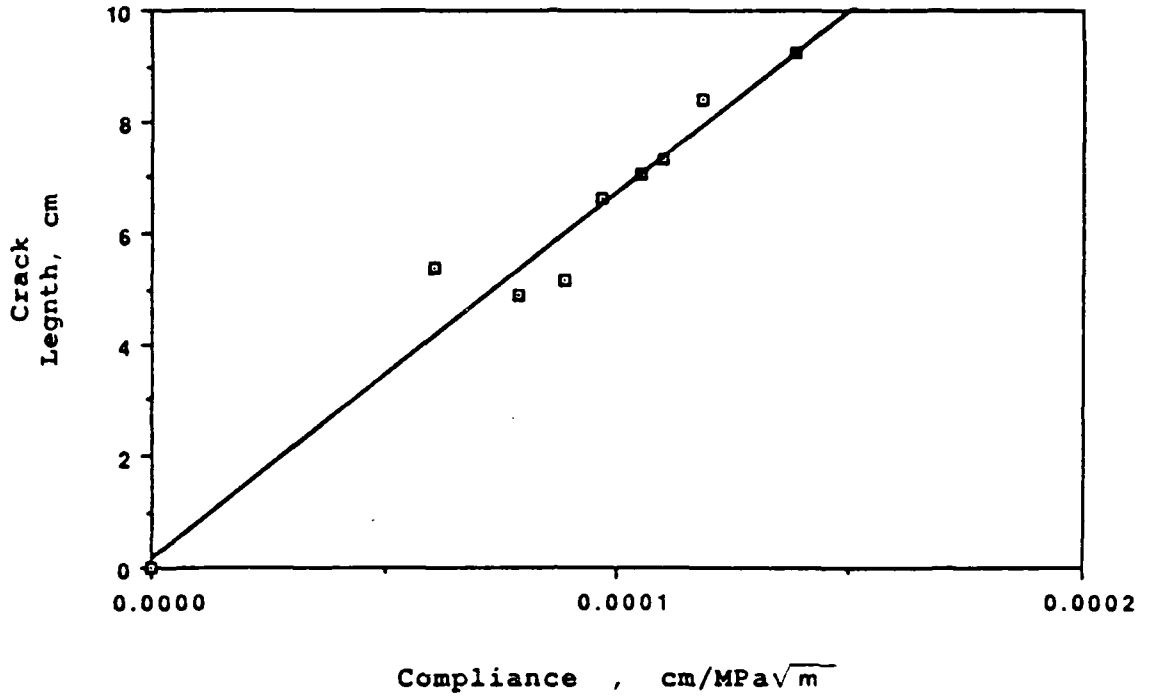

Fig. 4 Calibration curve for crack length vs compliance for 4340 steel (R_C 52). Experimental conditions: R = 0.5, f = 1 Hz, K_{max} = 35 MPa$\sqrt{m}$.

Figure 2b shows a photograph of the cell containing the sample, Pt-coated Ti grid counter electrodes, extensiometers, and reference electrode bridge.

2.3 Inhibitor Systems

A saturated xylene solution of tri-alkyl (C_8-C_{10}) ammonium complexes of the inhibiting anions borate, molybdate, dichromate and nitrite was prepared as described elsewhere.[10-12] This stock solution provided by NADC was diluted 10:1 with isopropanol for injection into the tip of a growing fatigue crack in Al 7075-T73 or a growing fatigue crack in 4340 steel. Injection was accomplished using a hyperdermic syringe and needle connected to flexible plastic tubing which could be placed near the crack tip. A 10:1 dilution with xylene was used to swab chromate conversion coated (CCC) Al 7075 panels or panels of Al 7075 with a conversion coating containing molybdate (CMT).

2.4 Experiments Designed to Probe the Role of Inhibiting Species on the Crack Tip Electrochemical Kinetics

The effect and electrochemical role of dilute aqueous anionic inhibitors (borate, molybdate, dichromate, and nitrite) on the CF of 4340 steel (R_C 52) were investigated using the fatigue admittance measurements as described in Sections 2.1 and 2.2. Previous efforts at NADC had shown that these anionic inhibitors synergistically diminish the CF of 4340 steel when they displace water at the crack tip as the alkyl ammonium salts in an organic phase. By using the fatigue admittance technique, small crack tip effects of the aqueous species can be evaluated. Accordingly, a full factorial experimental matrix was established using the inhibitor concentrations at high (0.01 M) and low (0 M) levels of concentration. The compounds used to make the solutions were reagent grade $Na_2B_4O_7 \cdot 10H_2O$, $Na_2MoO_4 \cdot 2H_2O$, $Na_2CrO_4 \cdot 4H_2O$ and $NaNO_2$. The experimental conditions used for these tests appear in Table 1.

Table 1

Test Conditions for Inhibitor Matrix

f = 1 Hz
R = 0.5
K_{max} = 35 MPa$\sqrt{m}$
Equilibrate to 5 h
Run polarization from E_o + 120 mV to -1000 mV at a rate of 1 mV/min
Monitor I_{ac}, I_{dc}, E, compliance
0.5 M NaCl aerated with/without 0.01 M inhibitor additions
One run performed with 10% DNBM/Xylene
4340 Steel (R_C 52)

After allowing the fatigue specimen to come to steady state by fatiguing for 4-5 h (Table 1), a potential sweep from 120 mV positive to the corrosion potential , E_o, to -1000 mV_{SCE} was performed while monitoring the fatigue current, I_{ac}, the dc electrochemical current, I_{dc}, and the compliance. These results yielded evaluation of the following parameters:

dA/dN_o - the crack growth rate at open-circuit potential, E_o

dA/dN_c - the crack growth rate in the cathodic region between -900 and -1000 mV

E_c - the corrosion potential of the crack tip taken as the potential of minimum I_{ac}

$I_{ac}(E_o)$ - the fatigue current at the open-circuit potential ($I_{dc} = 0$)

$I_{ac}(E_c)$ - the fatigue current at E_c

$1/R_{xp}$ - the observed slope of the polarization curve dI/dE at E_o which equals the inverse polarization resistance for a sufficiently slow potential sweep, but in this case provides a rough estimate of the relative corrosion rate for the boldly exposed surface.

2.5 Electrochemical Impedance Measurements

Electrochemical impedance measurements for 4340 steel rotating cylinder electrodes (IBM Model EC/219, r = 1380 rpm) and chemical conversion coated Al (CCC and CMT) were made using an optimized method as described elsewhere.[13] The system includes a PAR Model 13 potentiostat with a Model 276 computer interface which allows the gain of the current amplifier to be placed under computer control. A Solartron Model 1172 frequency response analyzer performed the frequency transforms of the respective current and potential fluctuations, and obtained their ratio which equaled the electrochemical impedance. The sinusoidal potential fluctuations were set at ±10 mV about the open-circuit potential. The impedance spectrum was determined stepwise typically from 100 kHz to 10 mHz under computer control. The current amplifier gain was set by the computer to optimize the measurement.[13] Resultant data were stored on magnetic tape and later transferred to the disk of a VAX 11/780 for archival storage and analysis.

The conversion coated Al alloys were prepared by the Naval Air Development Center (Vinod Agarwala), Warminster, PA. The cell used for measuring the impedance of the Al alloys included a plexiglass cylinder with an O-ring seal to the specimen surface, thereby allowing exposure of 23.8 cm^2 of the specimen surface to the 0.5 M NaCl test medium. A passivated 304 stainless steel electrode served as the counter electrode and a saturated calomel electrode (SCE) served as the reference electrode.

3.0 RESULTS

3.1 Fatigue Admittance of Al 7075-T73

3.1.1 Influence of Mechanical and Electrochemical Variables on I_{ac} for Al 7075-T73

Figure 5 shows the time dependence of I_{ac} for Al 7075-T73 in aerated 0. 5 M NaCl for a sinusoidally applied ΔK_{si} of 214 MPa $\sqrt{mm}$ and an R-value of 0.5 which equals the ratio of the minimum to the maximum stress intensity. As can be seen in Fig. 5, the fatigue current increases with time t giving a $t^{0.67}$ behavior over the observed time interval. I_{ac} increases as the crack length increases, but the rate of the increase decreases with time.

The time dependence of I_{ac} makes experimental evaluation of the role of the different mechanical variables difficult. Nevertheless, since the rate of change of I_{ac} decreases with time, experiments were performed to determine the dependence of I_{ac} on

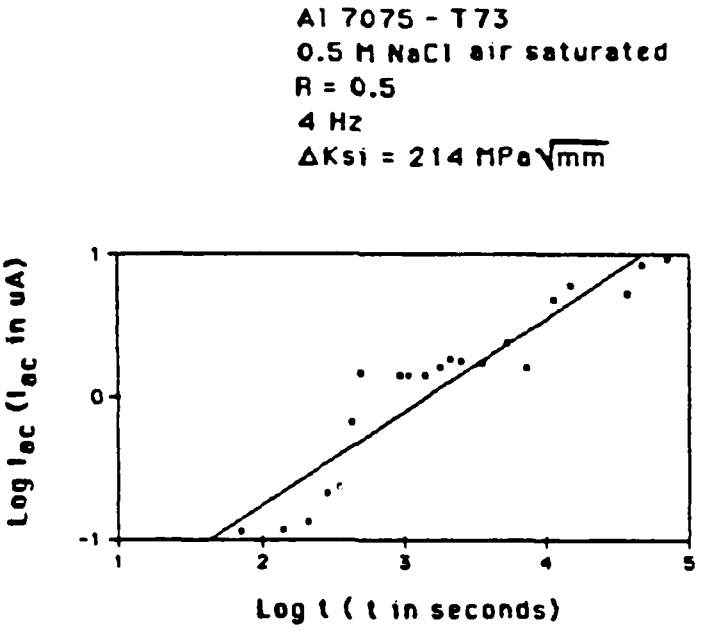

Fig. 5 Time dependence for the fatigue current, I_{ac}, for Al 7075-T73 in 0.5 M NaCl at 4 Hz.

R-ratio after a 20 h preconditioning at -745 mV vs SCE. The results for Al 7075-T73 at 4 Hz applied ΔK_{si} appear in Fig. 6. When the R-ratio is varied while keeping the mean load constant, I_{ac} increases with decreasing R-ratio. On the other hand, if the R-ratio is varied between 0.5 and 0.9, with a constant maximum K_{si}, I_{ac} remains more or less constant within experimental error. Figure 7 presents the data of Fig. 6 as a function of ΔK_{si}. As can be seen, I_{ac} increases with increasing ΔK when the mean load remains constant, but I_{ac} remains constant when the maximum K remains constant (Fig. 7). Clearly, the important stress intensity in CF for promoting the electrochemical reaction is the maximum K_{si}. Figure 8 and shows the increase in I_{ac} with increasing values of maximum K_{si}. I_{ac} depends on ΔK_{si} only inasmuch as the maximum K_{si} varies with ΔK_{si}. This shows that strain rate rather than the hydrodynamic conditions of crack opening and closing influences the electrochemical reactions at the crack tip and, hence, I_{ac}.

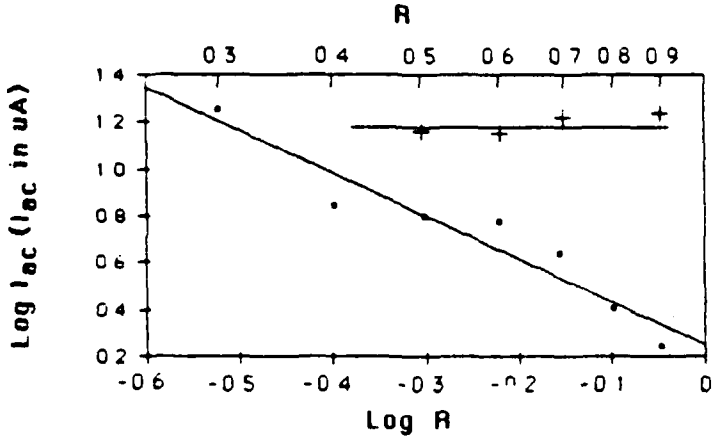

Fig. 6 R-ratio dependence for the fatigue current, I_{ac}, for Al 7075-T73 in 0.5 M NaCl at 4 Hz using constant mean load of 321 MPa$\sqrt{mm}$, or constant maximum amplitude of 427 MPa$\sqrt{mm}$.

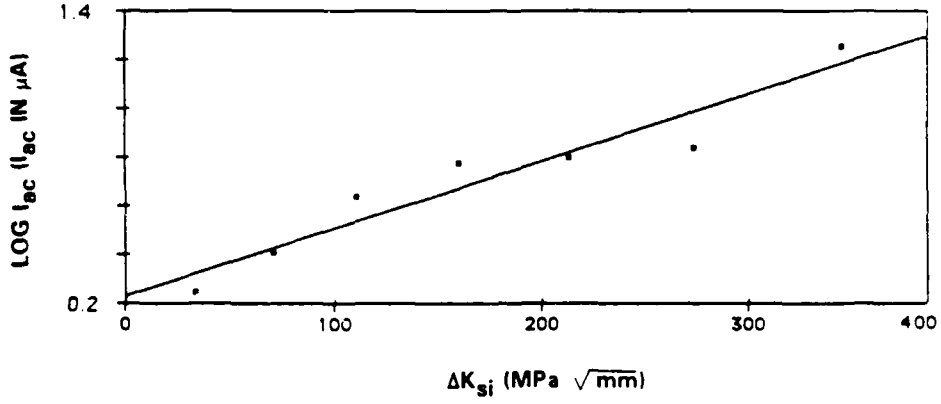

Fig. 7 I_{ac} as a function of ΔK_{si} for the data from Fig. 6.

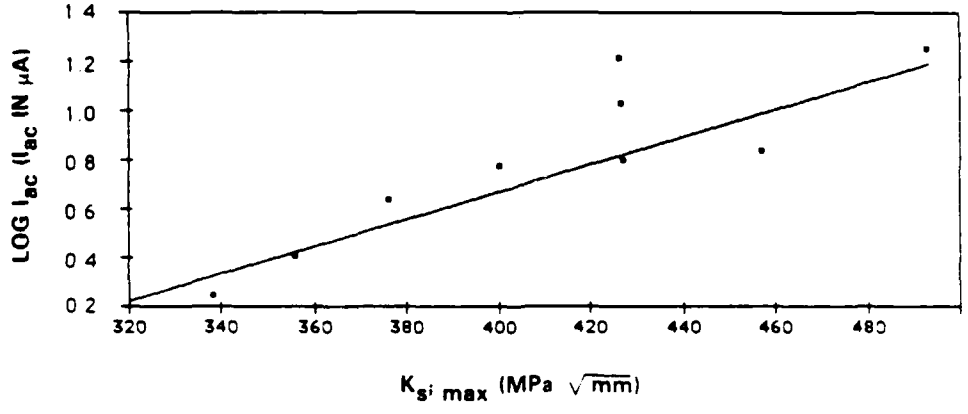

Fig. 8 I_{ac} as a function of $K_{si,max}$ for the data from Fig. 6.

3.1.2 Dependence of I_{ac} on Potential and the Presence of Inhibitor

Figure 9 shows the dependence of the fatigue current I_{ac} and the dc polarization current I_{dc} on applied potential for the Al 7075-T73 specimen before and after injecting the crack with the DNBM inhibitor that was dissolved in isopropanol (see Section 2.3). The experiments were performed after 450K cycles of fatigue of the specimen at open circuit in aerated 0.5 M NaCl by ramping the potential from slightly above the open-circuit potential, E_o, to more cathodic potentials at a rate of 0.1 mV/s while recording I_{ac} and I_{dc}.

As can be seen in Fig. 9, before injection of the inhibitor, E_o was defined as the point where I_{dc} equals zero. E_o occurs at -790 mV, but the minimum in I_{ac} which corresponds to the corrosion potential of the crack tip E_c occurs at -915 mV vs SCE. This suggests that at open circuit the crack tip is negative to the rest of the specimen by about 125 mV. After injecting the inhibitor in the crack tip, E_o increases to -750 mV. In

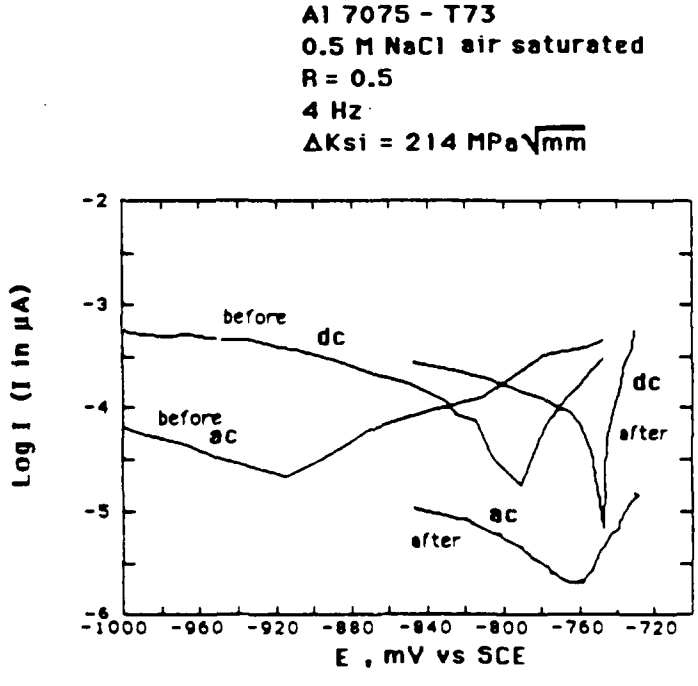

Fig. 9 Potential dependence for I_{ac} and I_{dc} for a fatigue specimen of Al 7075-T73 in 0.5 M NaCl at 4 Hz before and after injection of an isopropanol solution of DNBM inhibitor into the crack.

the presence of the inhibitor, I_{ac} shows a large increase in the potential where the minimum occurs from -915 mV before the addition of the inhibitor to -760 mV, only 10 mV more negative than E_o. Direct observation of E_c using microelectrodes placed ahead of a growing crack gives similar results for E_c.[14] In addition, the minimum for I_{ac} decreases by nearly an order of magnitude with the addition of the inhibitor. The most significant value of I_{ac} with regard to CF will not be the minimum value, I_{ac}^{min}, but rather the value at E_o, $I_{ac}(E_o)$. Most likely, $I_{ac}(E_o)$ relates directly to the electrochemical rate of anodic dissolution in the crack tip at the corrosion potential when E_c is less than E_o. As shown in Table 2, $I_{ac}(E_o)$ decreases by two orders of magnitude following injection of the inhibitor and remains low even after several 10^5 fatigue cycles.

Table 2

Summary of Fatigue Current Results for DNBM Inhibition Into the Crack

Cycles after Addition of DNBM, 10^3	E_a-E_o (mV)	Log($I_{ac}(E_o)$) (Amps)	Log($I_{ac}(E_c)$) (Amps)
0	-115	-3.6	-4.6
50	-12	-5.6	-6.1
209	-10	-5.9	-6.1
212	-8	-5.9	-6.1

3.2 Fatigue Admittance for 4340 Steel - Influence of Aqueous Anionic Inhibitors on the Crack Tip Electrochemical Reactions

Figures 10(a-c) show the potential dependence of the crack growth rate, dA/dN, the fatigue current, I_{ac} and the dc current, I_{dc}, which illustrates the nature of the raw data collected from an experiment with the conditions as presented in Table 2. The polarization of the specimen was performed about 4.5 h after conditioning by continuous fatigue at open circuit. The 4340 steel in 0.5 M NaCl without inhibitor shows a much higher crack growth rate as a function of potential than the sample in the solution containing the DNBM (Fig. 10a). Furthermore, dA/dN for the uninhibited specimen increases for potentials below -800 mV vs SCE. This cathodically produced acceleration in crack growth rate does not occur for the specimen with DNBM (Fig. 10a). I_{ac} for the

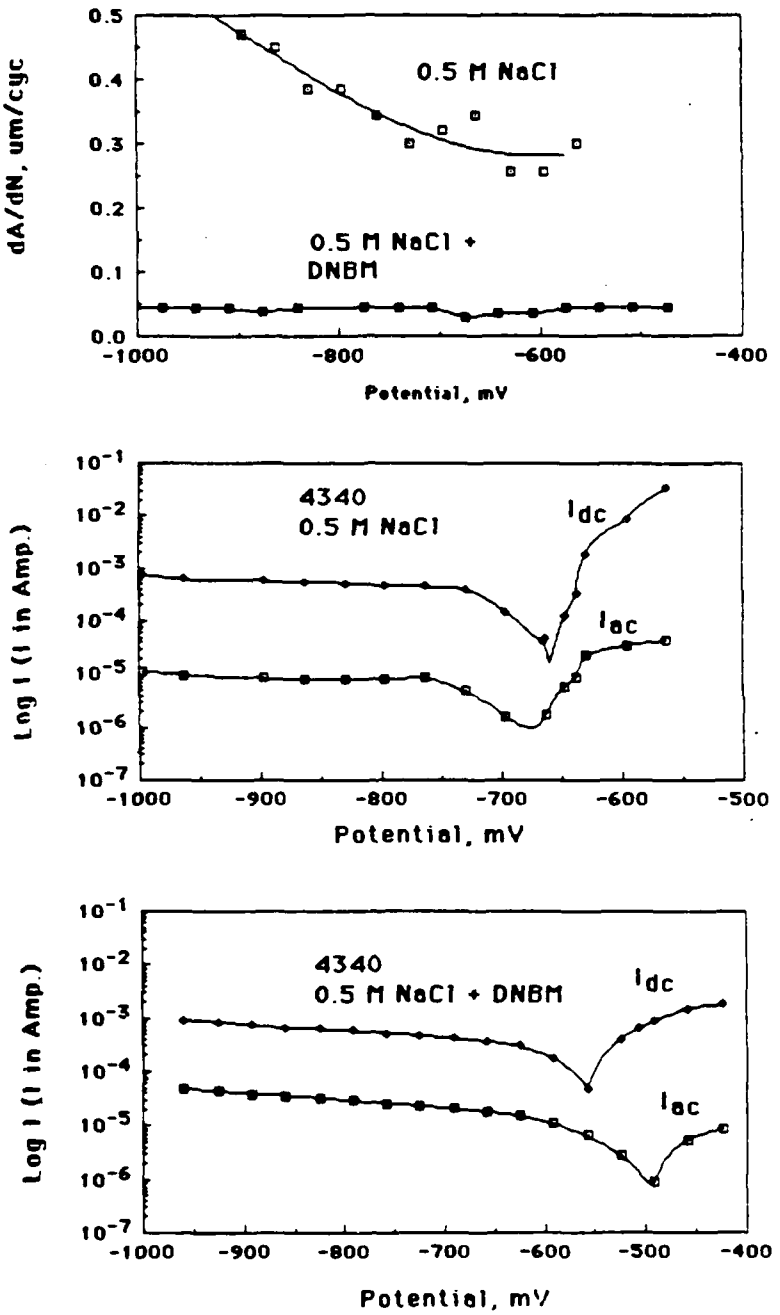

Fig. 10 Potential dependence for the (a) crack growth rate (5 m/s) for 4340 steel in 0.5 M NaCl with and without injection of DNBM inhibitor into the crack tip,(b) I_{ac} and I_{dc} vs potential in 0.5 M NaCl without DNBM, and (c) I_{ac} and I_{dc} vs potential in 0.5 M NaCl with DNBM. The conditions: f = 1 Hz, R-ratio = 0.5 and K_{max} = 34 MPa$\sqrt{m}$.

steel in 0.5 M NaCl shows a minimum at a potential which is about 20 mV more negative than E_o (I_{dc} = 0) (Fig. 10b). The potential for the minimum in I_{ac} equals E_c (corrosion potential of the crack tip). Note that in the DNBM-inhibited solution E_c is actually positive to E_o (Fig. 10c). The DNBM does not decrease I_{ac} at the potentials below E_c (Fig. 10c) as compared to the case where no inhibitor has been placed in the crack (Fig. 10b). However, DNBM produces a significant decrease on I_{ac} above E_c (Fig. 10c) as compared to the uninhibited specimen (Fig. 10b). These results demonstrate that the inhibitors are acting primarily to slow the anodic reaction in the crack tip.

Table 3 shows the results for the test matrix. The columns represent the observed parameters as defined previously in Section 2.4 and in Appendix I. The anionic inhibitors as present at a 0.01 M level in the bulk solution appear to have little influence on the crack growth rate at open circuit, dA/dN_o. Only when placed in the growing crack as the DNBM compound is there a significant decrease on the crack growth rate (Table 3 (I)). The water solvated inhibitors which increase the pH (above 8.0) have a significant influence in decreasing or eliminating the cathodic acceleration, dN/dN_c-dA/dN_o, of the fatigue cracking (Table 3 (II)). The DNBM inhibitor decreases the crack growth rate by a factor of 10 and increases the apparent open-circuit potential of the crack tip by 68 mV (Table 3 (II)). The role of the inhibitors in determing I_{ac} is not immediately clear. Since E_c for the DNBM is more positive than E_o, $I_{ac}(E_o)$ for the DNBM is negative. The inhibitors in the dilute aqueous environment appear to increase $I_{ac}(E_o)$ as compared to the case without inhibitors. Except for the borate + molybdate, the dilute aqueous inhibitors appear to have an accelerating influence on $I_{ac}(E_o)$ (Table 3 (III)). In the presence of borate, a buffering agent which maintains the pH above 9.0, all of the inhibitors appear to decrease the cathodic acceleration of the cracking, but have no influence at open circuit (Table 3 (III)).

Table 4 presents the results of the factorial analysis for the effects of the four water-solvated-inhibiting species (a = nitrite, b = chromate, c = molybdate and d = borate). Tabulated are the ratios of the mean square effects for the first (e.g., (a)) through fourth-order (abcd) effects to the estimated square error. The mean square effects were calculated as described in Appendix I and the errors were estimated from a duplicate run of the blank. The significance of the effects can be determined by comparing the calculated ratios in Table 4 to the F(1,1) value from statistical tables for a given confidence level. The F(1,1) values for 50, 75, 90, 95 and 99.5% confidence are 1, 5.83, 39.86, 161.4 and 16211, respectively.

Table 3

Summary of Results from Text Matrix

I Test Matrix

TEST(*)	Crack rate (Eo) dA/dNo um/cycle	Crack rate(-.9V) dA/dNc um/cycle	Cathodic accl dA/dNc-dA/dNo um/cycle	Corr Pot Ec mV	Shift Eo-Ec mV	Iac(Eo) uA	Iac(Ec) uA	1/Rc mho	pH
0000B	0.292	0.562	0.270	-656	21	5.0	1.56	0.0160	6.50
0001B	0.474	0.571	0.097	-407	113	36.0	8.00	0.0052	6.54
0010B	0.514	0.828	0.314	-583	43	21.6	3.60	0.0120	7.76
0011B	0.319	0.282	-0.037	-503	13	8.0	5.50	0.0065	8.78
0100B	0.253	0.357	0.105	-520	20	4.5	4.00	0.0200	8.99
0101B	0.750	0.301	-0.406	-354	77	17.5	6.45	0.0048	9.55
0110B	0.592	0.964	0.373	-588	-13	-6.0	4.00	0.0140	8.52
0111B	0.600	0.441	-0.160	-461	-33	-3.8	0.96	0.0240	8.42
1000B	0.302	0.259	-0.043	-545	20	32.0	28.00	0.0110	9.10
1001B	0.395	0.129	-0.267	-439	79	27.0	36.60	0.0048	9.17
1010B	0.302	0.238	-0.065	-585	44	13.0	4.00	0.0060	9.12
1011B	0.346	0.140	-0.205	-427	45	8.4	3.60	0.0034	9.10
1100B	0.297	0.137	-0.160	-500	31	5.1	7.50	0.0050	9.14
1101B	0.410	0.119	-0.292	-430	56	6.0	1.80	0.0060	9.10
1110B	0.444	0.204	-0.240	-534	21	4.7	3.30	0.0058	9.11
1111B	0.572	0.173	-0.400	-407	35	3.5	1.90	0.0030	9.80
DNBM	0.038	0.043	0.005	-515	-68	-10.0	2.20	0.0120	

II Single Inhibitors

TEST(*)	Crack rate (Eo) dA/dNo um/cycle	Crack rate(-.9V) dA/dNc um/cycle	Cathodic accl dA/dNc-dA/dNo um/cycle	Corr Pot Ec mV	Shift Eo-Ec mV	Iac(Eo) uA	Iac(Ec) uA	1/Rp mho	pH
No inhibitor	0.292	0.562	0.270	-656	21	5.0	1.56	0.0160	6.50
Nitrite	0.474	0.571	0.097	-407	113	36.0	8.00	0.0052	6.54
Dichromate	0.514	0.828	0.314	-583	43	21.6	3.60	0.0120	7.76
Molybdate	0.253	0.357	0.105	-520	20	4.5	4.00	0.0200	8.99
Borate	0.302	0.259	-0.043	-545	20	32.0	28.00	0.0110	9.10
All	0.572	0.173	-0.400	-407	35	3.5	1.90	0.0030	9.80
DNBM	0.038	0.043	0.005	-515	-68	10.0	2.20	0.0120	

III Borate Buffer

TEST(*)	Crack rate (Eo) dA/dNo um/cycle	Crack rate(-.9V) dA/dNc um/cycle	Cathodic accl dA/dNc-dA/dNo um/cycle	Corr. Pot Ec mV	Shift Eo-Ec mV	Iac(Eo) uA	Iac(Ec) uA	1/Rp mho	pH
No inhibitor	0.292	0.562	0.270	-656	21	5.0	1.56	0.0160	6.50
Borate	0.302	0.259	-0.043	-545	20	32.0	28.00	0.0110	9.10
Borate+nitrite	0.395	0.129	-0.267	-439	79	27.0	36.60	0.0048	9.17
Borate +dichr	0.302	0.238	-0.065	-585	44	13.0	4.00	0.0060	9.12
Borate + Moly	0.297	0.137	-0.160	-500	31	5.1	7.50	0.0050	9.14

(*) Test = abcdB where
Borate at 0.01 M a = 1
Molybdate at 0.01 M b = 1
Dichromate at 0.01 M c = 1
Nitrite at 0.01 M d = 1

Table 4

Ratio of Mean Squares

dA/dNo um/cycle	dA/dNc um/cycle	cath. accel um/cycle	Eo mV	Eo-Ec mV	Iac(Eo) uA	Iac(Ec) uA	1/Rp mho	
7.39	18.95	12.08	**1145.40**	9.57	32.35	4.90	62.65	a
2.60	6.81	0.19	54.85	16.76	**438.38**	**280.98**	0.32	b
9.26	0.96	3.78	120.31	8.27	**893.26**	**232.18**	18.55	c
5.15	82.53	12.12	41.04	1.98	17.75	**173.12**	**210.11**	d
7.91	9.82	0.05	9.57	17.54	**203.42**	13.56	59.05	ab
3.78	0.18	0.49	10.36	0.52	3.20	36.69	19.46	ac
0.13	6.87	2.03	25.31	0.00	112.63	2.76	6.87	ad
2.25	7.93	0.35	17.80	1.81	12.69	143.22	24.30	bc
0.00	3.67	0.80	24.69	7.91	0.44	**190.10**	23.69	bd
0.46	0.02	0.12	9.96	2.16	0.47	**185.30**	49.26	cd
0.02	0.02	0.00	17.80	2.07	61.43	9.53	9.20	abc
1.67	0.48	0.86	0.94	0.00	8.34	2.54	0.84	acd
6.76	10.58	0.16	98.13	4.13	**180.57**	1.78	60.08	abd
0.54	3.99	1.69	27.89	0.47	**189.41**	**209.74**	8.09	bcd
0.30	0.17	0.18	15.26	0.00	82.13	12.69	45.44	abcd

a = nitrite
b = dichromate
c = molybdate
d = borate
bold numbers indicate significant effects at the 95% level

As can be seen for the bulk electrolyte state, the anions at the 0.01 M concentration level appear to have no significant effect on dA/dN_o, the crack growth rate at open circuit, as they do in the form of the DNBM formulation which decreases the crack growth rate in this environment by nearly a factor of 10. The analysis does show, however, that the borate plays a statistically significant role in decreasing dA/dN_c, the crack growth rate between -900 and -1000 mV at a confidence level of 90%. Borate also has a significant influence on the corrosion of the boldly exposed surface as it has a significant effect on the inverse of the observed corrosion resistance $1/R_{xp}$ at the 95% level. The molybdate and dichromate inhibitors (b and c) have significant effects at the 95% level on the kinetics of the crack tip as determined by the observed $I_{ac}(E_o)$ and $I_{ac}(E_c)$. The results show some higher order effects for nitrite and dichromate (ab), nitrate-dichromate-borate (abd) and dichromate-molybdate-borate (bcd) on $I_{ac}(E_c)$ and $I_{ac}(E_o)$ and also higher order contributions to $I_{ac}(E_c)$ (Table 4).

Using the significant effects from Table 4, multiple regression analyses were performed. The multiple regression analysis fits the data to the equation:

$$Y = \text{constant} + \left(\sum_{i=a,b,c,d} k_i[i]\right) + \left(\sum_{\substack{i\neq j \\ i=a,b,c,d}} k_{ig}[i]\ [j]\right)$$

$$+\left(\sum_{\substack{i\neq j\neq k \\ i=a,b,c,d}} k_{ijk}[i]\ [j]\ [k]\right) + k_{abcd}[a]\ [b]\ [c]\ [d] \quad ,$$

where Y is a given response (e.g., dA/dN_o). Regression analyses were performed using only the significant first and higher order effects for the responses dA/dN_c, E_o, $I_{ac}(E_o)$, $I_{ac}(E_c)$, $1/R_{xp}$, and pH. The results appear in Table 5. Borate has a very significant effect in decreasing the cathodic cracking rate dA/dN_c. The borate increases pH, thereby lowering the rate of hydrogen penetration at the cathodic potential, so as to lower the rate of hydrogen embrittlement (HE).

Both molybdate and borate have a significant first-order influence on increasing the corrosion potential, E_o, of the boldly exposed specimen by forming films which block the diffusion-controlled oxygen reduction. Higher order effects on E_o had zero coefficients within the standard error. The dichromate and molybdate inhibitors were significant in decreasing the fatigue current observed at open circuit. Higher order effects on $I_{ac}(E_o)$ were insignificant within the standard error.

The $I_{ac}(E_c)$ response to the inhibitors showed significant negative second-order effects (borate and molybdate, and borate and dichromate). However, a third-order effect of borate, dichromate and molybdate appeared to be positive. The physical significance of this is not clear at this time. Possible interaction between the chromate and molybdate which reduces their respective activity could account for this effect. Borate also appears to have a positive effect on $I_{ac}(E_c)$ (Table 5).

Borate decreases the corrosion rate of the bulk specimen as measured by $1/R_{xp}$ (Table 5), which is no doubt a pH effect. Both borate and molybdate increase the pH of the medium (Table 5).

The correlations between the different responses appear in Figs. 11-15. Each experiment provided one point in each of the plots (Figs. 11-15). Figure 11 shows the negative shift in the corrosion potential of the crack tip, E_o-E_c, vs the CF rate at open circuit, dA/dN_o. The shift in E_c to more negative values occurs with increasing crack growth rate. As E_o-E_c increases, so does the fatigue current at the corrosion potential of the bulk specimen, $I_{ac}(E_o)$ (Fig. 12).

A remarkably good negative correlation (-250 mV/μm/cycle) occurs between the open-circuit potential of the boldly exposed surface (E_o) and the cathodic acceleration of the CF, dA/dN_c-dA/dN_o (Fig. 13). dA/dN_o shows a slight increase with E_o (195 mV/μm/cycle), while dA/dN_c shows a decrease with increasing E_o (-138 mV/μm/cycle). This suggests that the passivating inhibitors may also slow the hydrogen entry into the steel at cathodic potentials. A similar conclusion was recently drawn by Scully.[15]

There also appears to be a correlation of the corrosion rate of the boldly exposed surface as measured by $1/R_{xp}$ with the CF parameters E_o-E_c and dA/dN_c-dA/dN_o (Figs. 14-15). $1/R_{xp}$ decreases with increasing shift of E_c to more negative potentials (Fig. 14) and increases with increasing cathodic acceleration of CF (Fig. 15).

In general, these results demonstrate that inhibitors in the bulk solution at the 0.01 M level show only very small effects, if any, on the cracking of 4340 steel at open circuit. The Mo and Cr oxy-anions, however, significantly decrease the anodic dissolution associated with the fatigue cycle, but not sufficiently to lower the CF rate substantially, since it primarily results from hydrogen permeation, as evidenced by the increased CF rate with decreased potential in the absence of the inhibitor (Fig. 10a). Only the borate ion which buffers the solution to a pH above 9 decreases the cracking rate, but only at cathodic potentials. The results presented here show that in the absence of corrosion inhibitors, cathodic polarization below -900 mV accelerates rather than inhibits CF. Note that the experimental conditions are such that the cracks are long and well into the propagation stage. It must be emphasized that the inhibitors, in the absence of

Table 5

Regression Analysis

dA/dN_C (μm/cycle)		I/R_p (mho)	Coefficient
const	0.54 ± 0.06	const	0.013 ± 0.002
[borate]	-0.36 ± 0.09	[borate]	-0.007 ± 0.003
E_o (mV)		pH	
const	-586 ± 19	const	7.691 ± 0.3
$[MoO_4^=]$	43 ± 22	[borate]	1.14 ± 0.4
[borate]	132 ± 23	$[MoO_4^=]$	0.88 ± 0.4
	*		
$I_{ac}(E_o)$ (μA)			
const	25.21 ± 4		
$[M_oO_4^=]$	-17 ± 5		
$[Cr_2O_7^=]$	-10.5 ± 6		
	*		
$I_{ac}(E_c)$ (μA)			
const	5.4 ± 2		
[borate]	26.9 ± 3		
[borate][$MoO_4^=$]	-26.8 ± 4		
[borate][$Cr_2O_7^=$]	-27 ± 4		
[borate][$Cr_2O_7^=$][$MoO_4^=$]	26± 4		

* Higher order coefficients ~ 0 within error.

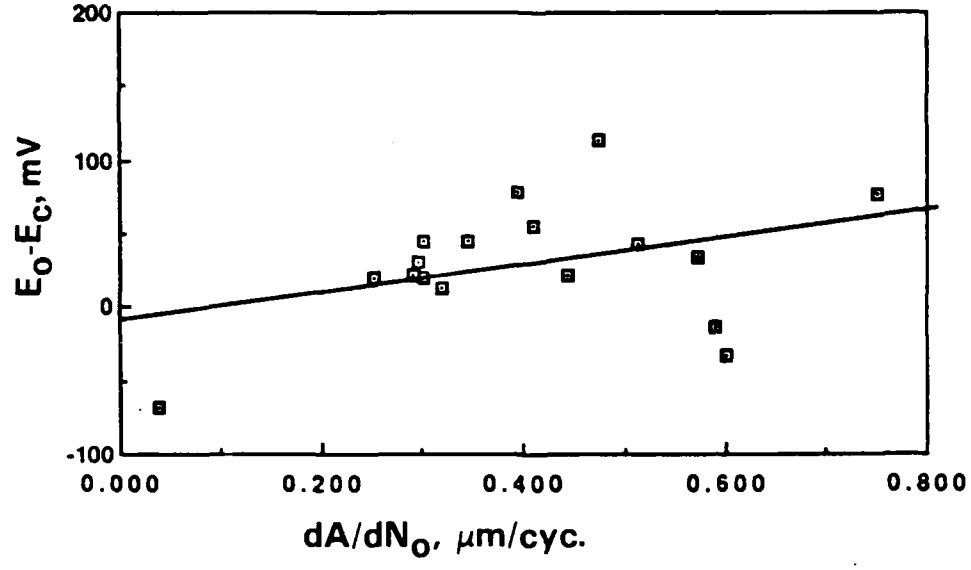

Fig. 11 E_o - E_c plotted as a function of dA/dN_o for 4340 steel and the conditions of Table 1.

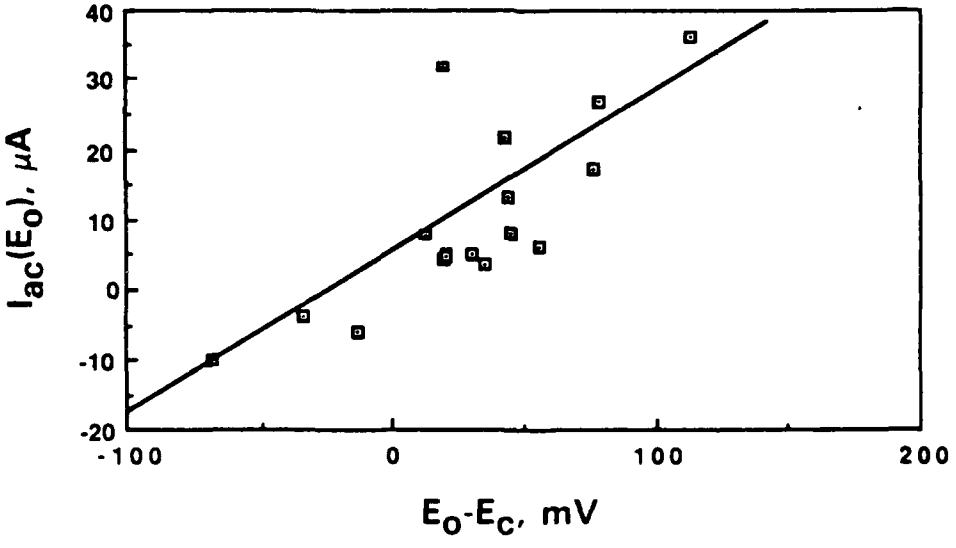

Fig. 12 $I_{ac}(E_o)$ plotted as a function of E_o-E_c for 4340 steel and the conditions of Table 1.

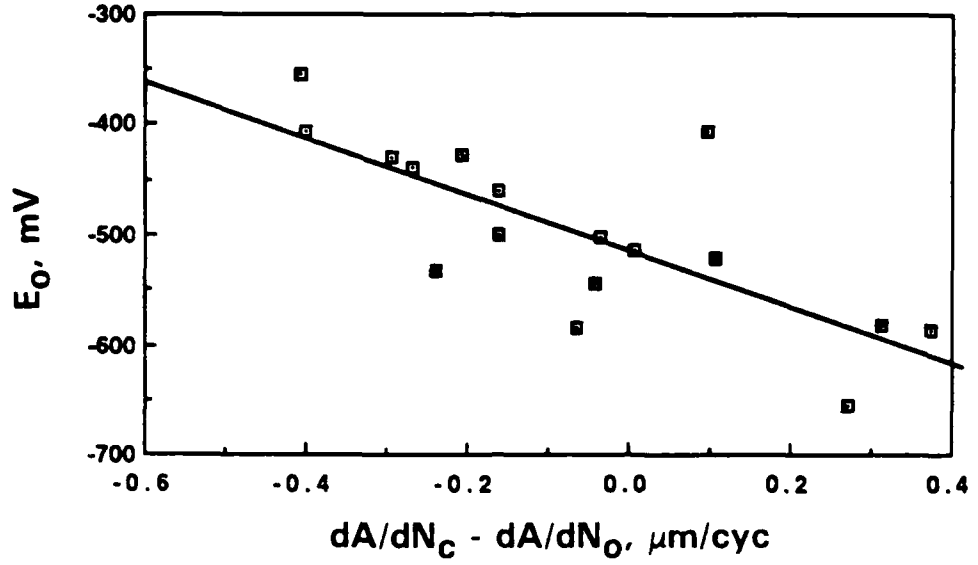

Fig. 13 E_o plotted as a function of $dA/dN_c - dA/dN_o$, the difference between the CF rate at -900 mV_{SCE} and the corrosion potential, for 4340 steel and the conditions of Table 1.

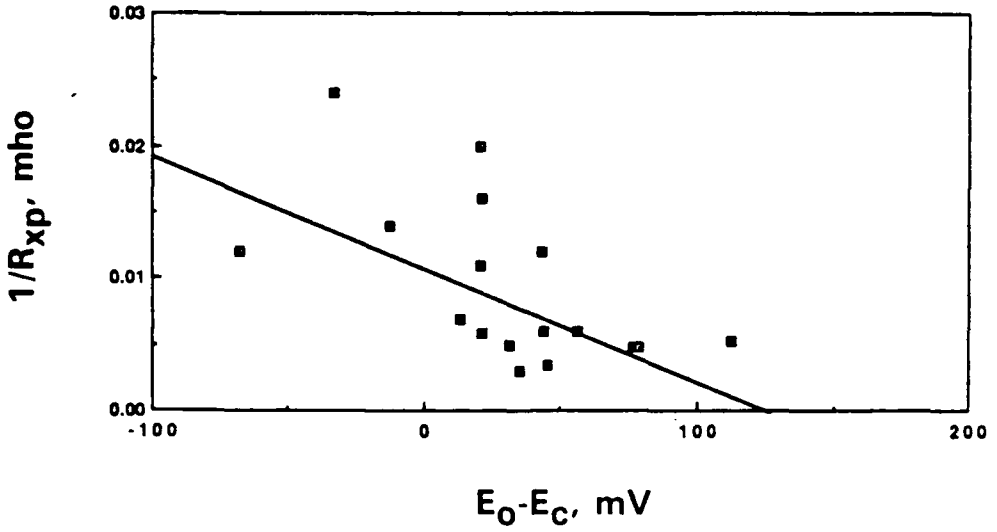

Fig. 14 $1/R_{xp}$ plotted as a function of E_o-E_c for 4340 steel and the conditions of Table 1.

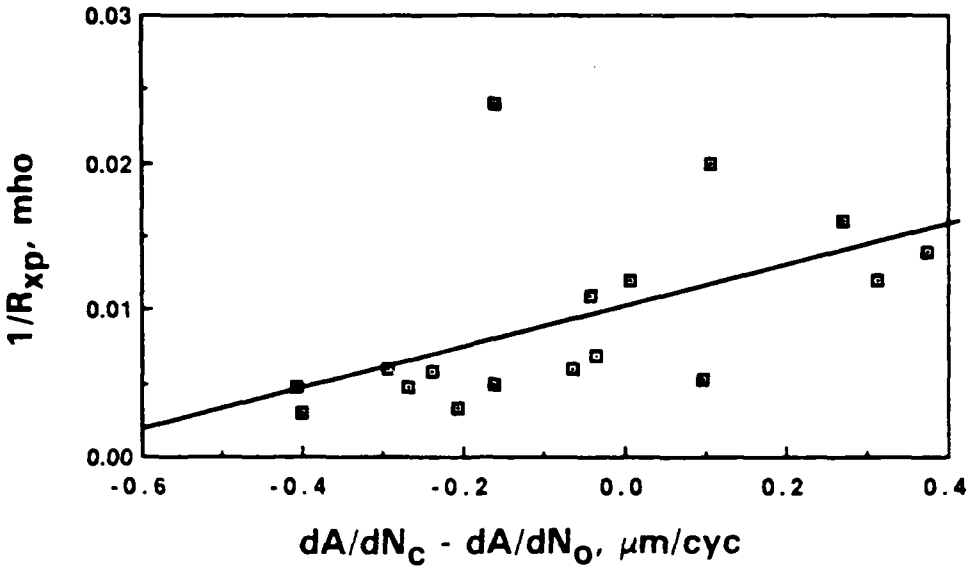

Fig. 15 $1/R_{xp}$ plotted as a function of dA/dN_c-dA/dN_o, the difference between the CF rate at -900 mV_{SCE} and the corrosion potential, for 4340 steel and the conditions of Table 1.

hydration and complexed in a low surface energy water displacing organic phase by a phase transfer catalyst, decrease the cracking rate by a factor of 10 or more for all potentials.

3.3 Evaluation of Corrosion Protection by Inhibitors and Coatings

As part of the technology transfer of the impedance techniques to NADC, which is part of this project, the Project Manager, Dr. Vinod Agarwala, spent time in February and October, 1986 at the Science Center. The use of electrochemical impedance spectroscopy (EIS)[16-19] for the evaluation of corrosion protection measures such as the use of inhibitors,[18,20] polymer coatings,[21-24] and surface treatments of Al alloys (conversion coatings, anodizing),[24,25] and the experimental approach developed at the Science Center[13] were discussed. Dr. Agarwala also witnessed the measurement of the impedance during corrosion fatigue of Al 7075 in NaCl, which is the main task of this project.

The application of EIS to the evaluation of corrosion protection schemes was illustrated for a mixed inhibitor developed by NADC and for conversion coatings on Al 2024 and 7075. Impedance spectra were collected with a computerized system[13] which uses a Solartron frequency response analyzer, Model 1174, and a PAR potentiostat, Model 173, with a Model 276 interface (see Section 2.5).

3.3.1 Evaluation of a Mixed Inhibitor for Steel

For the evaluation of the mixed inhibitor on steel in 0.5 M NaCl (open to air), a rotating cylinder electrode (RCE) was used.[20] The inhibitor was applied by repeated dipping of the steel sample into a solution of the inhibitor dissolved in toluene, followed by drying in air. Figure 16 shows a comparison of EIS data in the form of Bode-plots for a rotating (r = 1380 rpm) and a stagnant electrode for two exposure times. These two cases were studied to determine the possibility of transport of the inhibitor away from the surface. The spectra are characterized by a single time constant with a broad maximum. In the capacitive region, a slope between 0 and -1, is observed. Ideal capacitive behavior requires a slope of -1. This type of spectrum would correspond to a depressed semicircle in a Nyquist-plot. After 5 h, very little difference between the rotating and the stagnant electrode is observed in the capacitive region. However, the dc limit, which corresponds to the polarization resistance R_p, is about 60% lower for the rotating electrode. This increase of corrosion rate could be due to the increased transport of oxygen to the surface, but it could also result from removal of the inhibitor due to rotation, or it could result as a combination of both possibilities. That inhibition takes place in both cases is indicated by the increase of R_p to 700 Ω-cm^2 from the previously determined value of about 100 Ω-cm^2 in inhibitor-free NaCl, as shown in the Nyquist presentation ($-Z''$ vs Z') in Fig. 17. After 23 h, a marked difference in the spectra has occurred (Fig. 16). The phase angle for the rotating electrode has a very broad maximum, and the slope of the impedance curve in the capacitive region is much lower. The difference in the R_p values between the rotating and stagnant electrodes has increased somewhat.

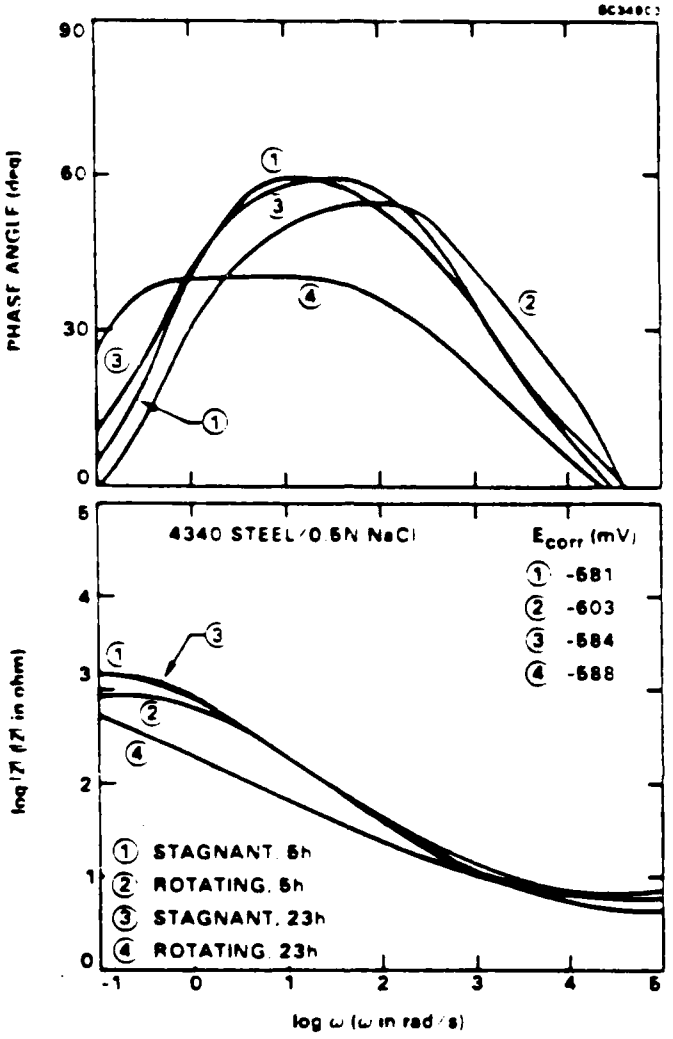

Fig. 16 Bode-plots for rotating and stagnant inhibited steel cylinder electrodes in 0.5 M NaCl after exposure times of 5 and 23 h.

Important information can be obtained by a comparison of the corrosion potential E_o for the two electrodes. Contrary to the standard case in inhibitor-free solutions where E_o increases with rotation speed due to the increased mass transport of O_2,[20] E_o remains more or less constant. This behavior is typical for interphase inhibition as discussed by Lorenz and Mansfeld[26] and is illustrated by the case of a mixture of phosphonic acid/fatty amine as the inhibitor for steel.[20] Together with the observed shape of the impedance spectra especially after 23 h (as shown in Fig. 17), this result suggests that the inhibitor-covered surface corresponds to that described by the "blocked surface

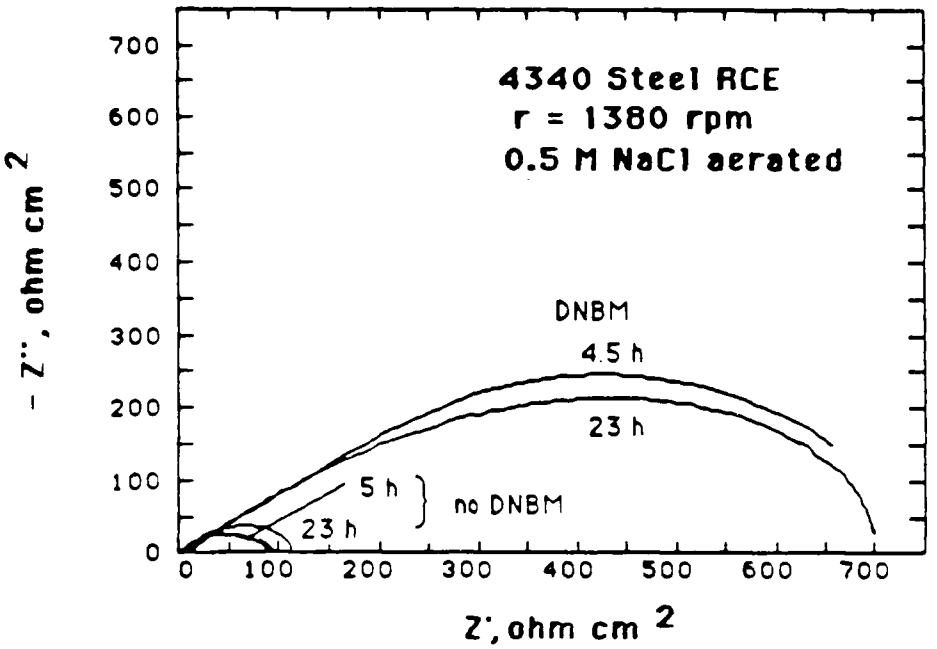

Fig. 17 Nyquist plots for 4340 steel RCE with and without DNBM at different exposure times.

model", which has been developed in collaboration with Lorenz and Juettner in Germany and Schmidt in Switzerland. Figure 18 shows the equivalent circuit for this model and a Nyquist plot of simulated impedance plots for different Nernst diffusion layer dimensions, as determined by rate of electrode rotation.

According to the blocked surface model, the surface of the steel is considered to be covered partially with corrosion products at sites where the anodic process occurs. The reduction of oxygen takes places in pores of the corrosion product layer. Interphase inhibitors function by blocking these pores and becoming incorporated in the surface layer. Due to this structure of the surface layer, changes in the hydrodynamic conditions do not have the marked effect on E_o and the corrosion rate that would be expected from the simple Levich theory for "clean" surfaces.

A computer program which minimizes the difference between the observed and calculated Nyquist plot of the impedance spectrum can be used to estimate the parameters of the model. Figure 19 shows the results of the computerized fit (solid lines) after 5 h for 4340 steel RCE with and without the DNBM inhibitor. Since only a little experience has been gained at this time in regard to extracting the parameters of the model using the computer fitting, it is not clear that the computerized fit represents a unique

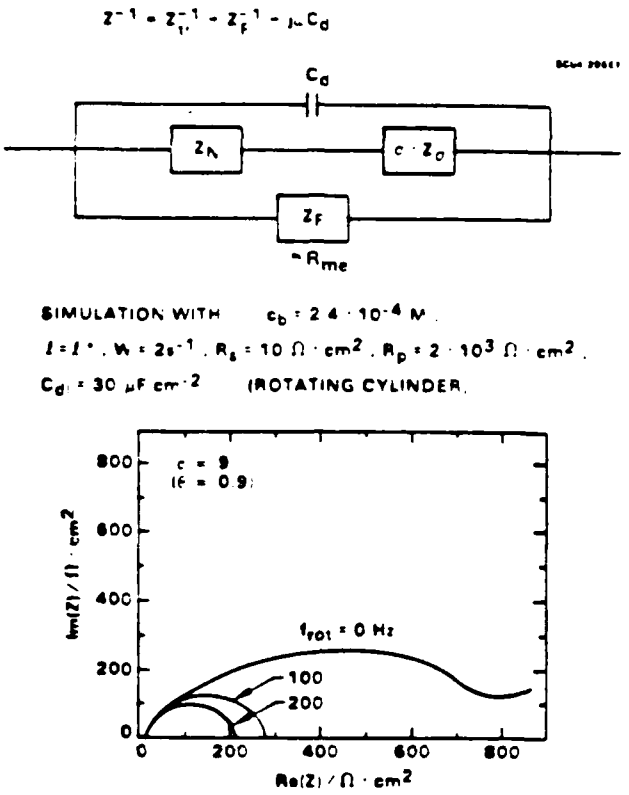

Fig. 18 Equivalent circuit and simulated impedance plots for the blocked surface model.

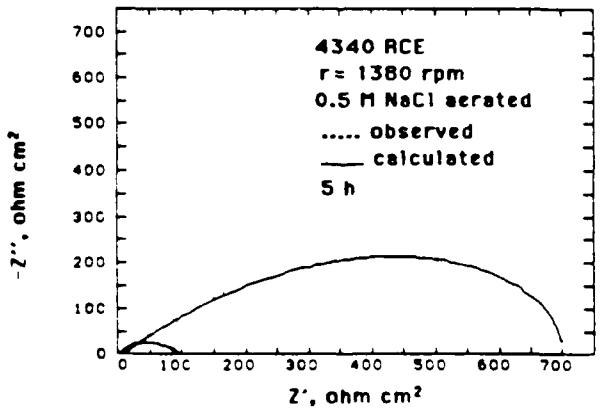

Fig. 19 Computerized fit of blocked surface model for the results from the 4340 steel RCE with and without DNBM at 5 h.

evaluation of the parameters. Nevertheless, the currently determined "best fit" values for R_d, R_d*, and R_p for the steel with and without inhibitor appear in Table 6. R_d and R_d* relate directly to the homogeneous and inhomogeneous diffusion impedances, respectively, according to:

$$Z_N = R_d h(\omega)$$

$$Z_\sigma = R_d^* h^*(\omega)$$

where $h(\omega)$ and $h^*(\omega)$ are complex functions of frequency discussion of which is beyond the scope of this report. R_{me} is inversely proportional to $\partial i_{anodic}/\partial E$ at E_o, where i_{anodic} is the current density for anodic dissolution. Clearly, the inhibitor dramatically increases all of these values which are related to the electrochemical rates involved in the corrosion of the metal.

Table 6

R_d, R_d* and R_{me} for 4340 Steel RCE With and Without DNBM Corrosion Inhibitor

Parameter	Inhibited	No Inhibitor
R_d, Ω-cm^2	1630	99
R_d*, Ω-cm^2	5360	1310
R_{me} Ω-cm^2	700	100

3.3.2 Evaluation of Conversion Coatings for Aluminum 2024

EIS is also a very efficient tool for the evaluation of high impedance protective coatings such as conversion coatings and anodized surface layers on Al alloys.[25] A comparison has been made for Al 2024 with the commercial Alodine 1200 conversion coating and a treatment which contains Mo (CMT) developed at NADC. The tests were conducted in 0.5 N NaCl (open to air) at pH = 4 and in neutral solutions. A comparison of Bode plots in these two solutions for two exposure times is given in Figs. 20 and 21. At pH = 4, two time constants are observed for very short exposure times, but only one time constant remains after 21 h. The CMT coating seems to be thinner as reflected by the higher capacitance. The inductive behavior for the CMT coating, which is evidenced by

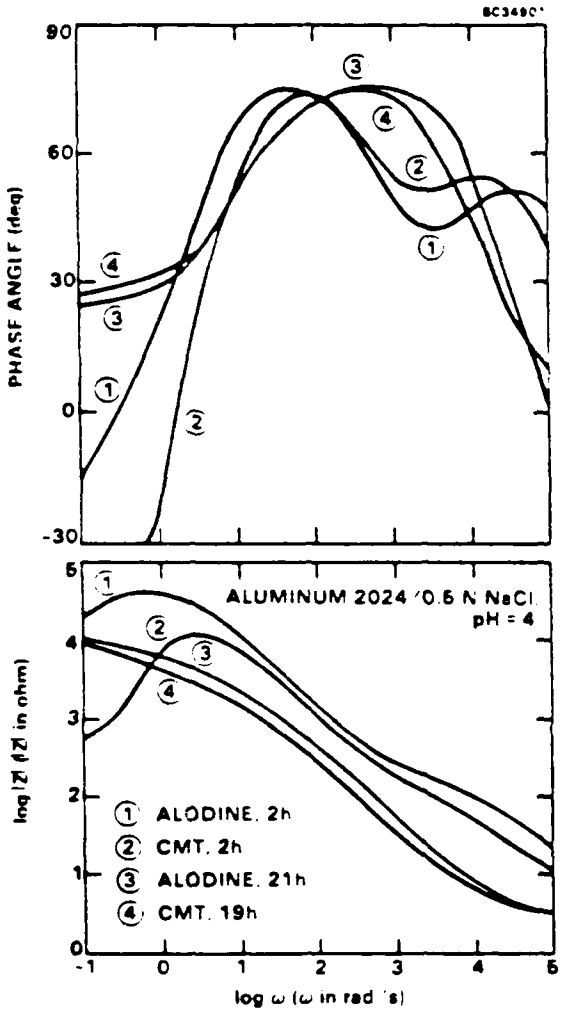

Fig. 20 Bode-plots for Al 2024 with two different conversion coatings during exposure to 0.5 M NaCl, pH = 4.

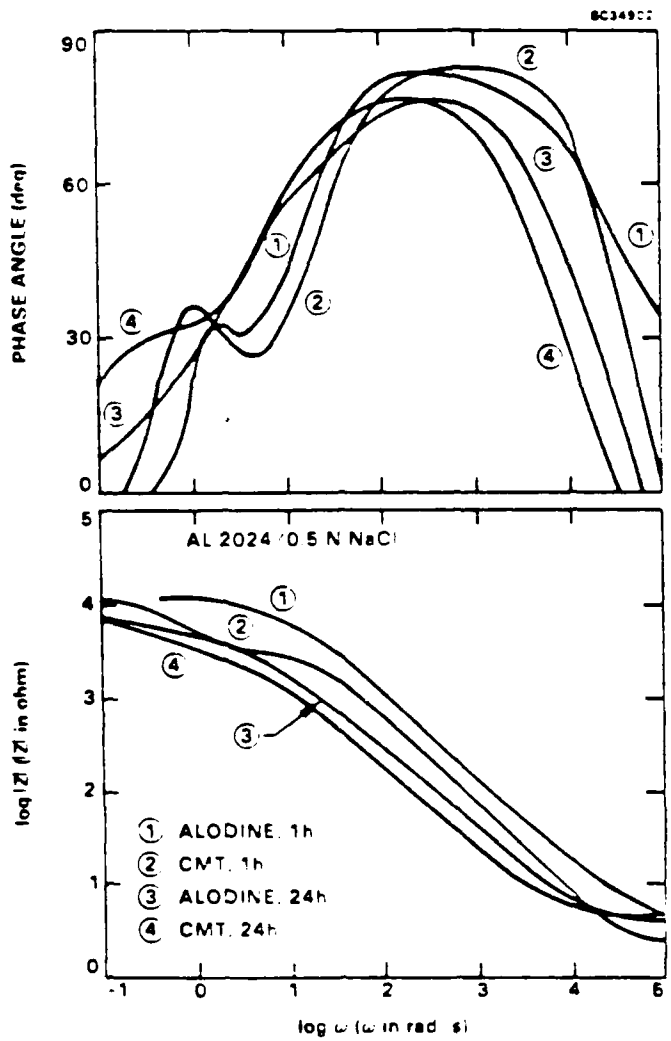

Fig. 21 Same as Fig. 20, but at neutral pH.

the decrease of the impedance with decreasing frequency at the lowest frequencies and the negative phase angle, could be due to localized corrosion in the form of pitting and/or crevice corrosion. Similar behavior has been observed earlier[27] for an anodized Al/SiC metal/matrix composite where crevice corrosion had occurred under a seal. The dc limit which exceeds 10^4 Ω (2×10^5 Ω-cm^2) indicates the improved corrosion resistance of both samples of conversion coated Al 2024.

For neutral NaCl, only one time constant occurs at high frequencies (Fig. 21), as observed earlier at the Science Center in a study in which a comparison was made of different conversion coatings (Alodine 600, 1200 and 1500) and Al alloys (2024, 6061 and 7075). For the CMT coating, a second time constant can be seen at low frequencies, which again could be due to localized corrosion. The dc limit of about 2×10^5 Ω-cm^2 reflects the corrosion protection of the coating. For bare Al 2024, R_p-values of about 10^3 Ω-cm^2 have been determined earlier in 0.5 N NaCl.[21]

3.3.3 Impedance of Conversion-Coated and Inhibitor-Treated Al 7075

Al alloy surfaces are often protected against corrosion by chemical conversion coatings which often must be conducting as well as corrosion resistant. A need exists to improve the corrosion resistance of conversion-coated Al without increasing the surface resistivity. One way this can be accomplished is by incorporating corrosion inhibitors in the conversion-coated film. In investigating the efficiency of different processes for improving the corrosion resistance of conversion-coated Al, one requires a rapid method for evaluating the processed surfaces. Electrochemical impedance methods are particularly suited for evaluating the corrosion resistance of conversion-coated Al alloys.

Figure 22 shows the Bode plots for the impedance of untreated polished Al 7075 between 1-46 h immersion in aerated 0.5 M NaCl. The impedance spectra are characterized by a plateau equal to a charge transfer resistance of 10^4 Ω-cm^2 at frequencies between 1 and 10 rad/s and a ω^{-1} region above 10 rad/s, due to the film capacitance. Below 1 rad/s, the impedance increases slowly with frequency. This region of the spectrum for bare alloys has been attributed recently to pitting.[29] In time, the film grows, as evidenced by an apparent decrease in the capacitance (increase in impedance for frequencies above 10 rad/s). Little change in the transfer resistance occurs.

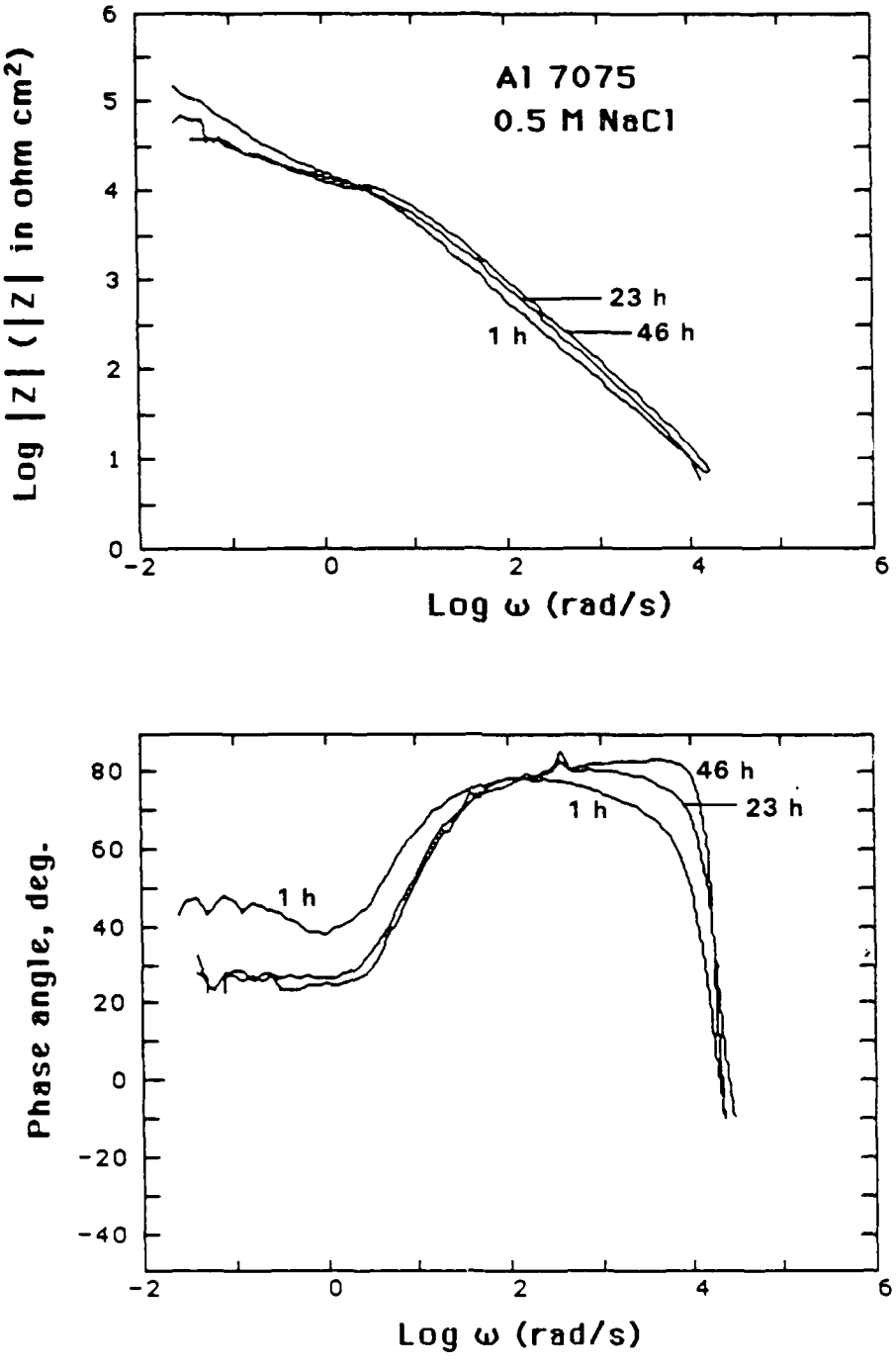

Fig. 22 Bode plots for Al 7075 in aerated 0.5 M NaCl after 1, 23 and 46 h.

The chromate conversion-coated (CCC) Al 7075 (Fig. 23) initially shows a much higher impedance and a more complicated spectrum. Two time constants appear in the initial spectrum (Fig. 23a). The high frequency part disappears with time of exposure. Initially, the polarization resistance (dc limit of the impedance) for the CCC Al 7075 is over 10^5 Ω-cm^2, but after 24 h, it decreases to about 2×10^4 Ω-cm^2, close to that for the untreated Al 7075. For all times, an apparent inductive effect appears which may be due to pitting.

In the case where the CCC-treated alloy is wiped with a solution of 10% DNBM in xylene solution before exposure to 0.5 M NaCl, the impedance spectrum does not change over 218 h (Fig. 24), and the polarization resistance remains above 3×10^6 Ω-cm^2, which represents a 100-fold increase in the corrosion resistance of the material, as compared to the CCC alloy without the DNBM.

The chromate conversion coating containing Mo compounds (CMT) initially shows an impedance spectrum with a dc limit or polarization resistance, R_p, that exceeds that for the CCC-treated specimen by a factor of 5 (Fig. 25). This cannot be attributed to the presence of a thicker film on the CMT specimen since the initial capacitances for the two specimens are nearly the same at 2.1 μF/cm^2 for the CMT and 1.7 μF/cm^2 for the CCC specimen. As for the CCC-coated specimen, the R_p for the CMT specimen decreases from 4.4×10^5 Ω-cm^2 at 1 h to 4.1×10^4 Ω-cm^2 at 23 h. After 23 h, the specimen was removed from the 0.5 M solution, rinsed and dried. Ten percent DNBM solution was then wiped on the surface before placing the sample back in the 0.5 M NaCl solution. Subsequently measured impedance spectra showed that the surface "healed", as determined by an increase in R_p to 10^6 Ω-cm^2 at 26 h and a further increase to over 3×10^6 Ω-cm^2 at 242 h (Fig. 25).

The best performance for conversion-coated and treated Al 7075 was obtained for CMT-coated and DNBM-treated alloy. Except for an anomalous drop in $|Z|$ at low frequency observed at 48 h and attributed to an artifact of over polarization, the impedance spectra for this specimen remained constant for more than 339 h (Fig. 26). The polarization resistance remained at approximately 10^7 Ω-cm^2, which represents a 100-fold improvement in the corrosion resistance of the alloy over the CCC-treated material and a 1000-fold improvement over the polished untreated alloy.

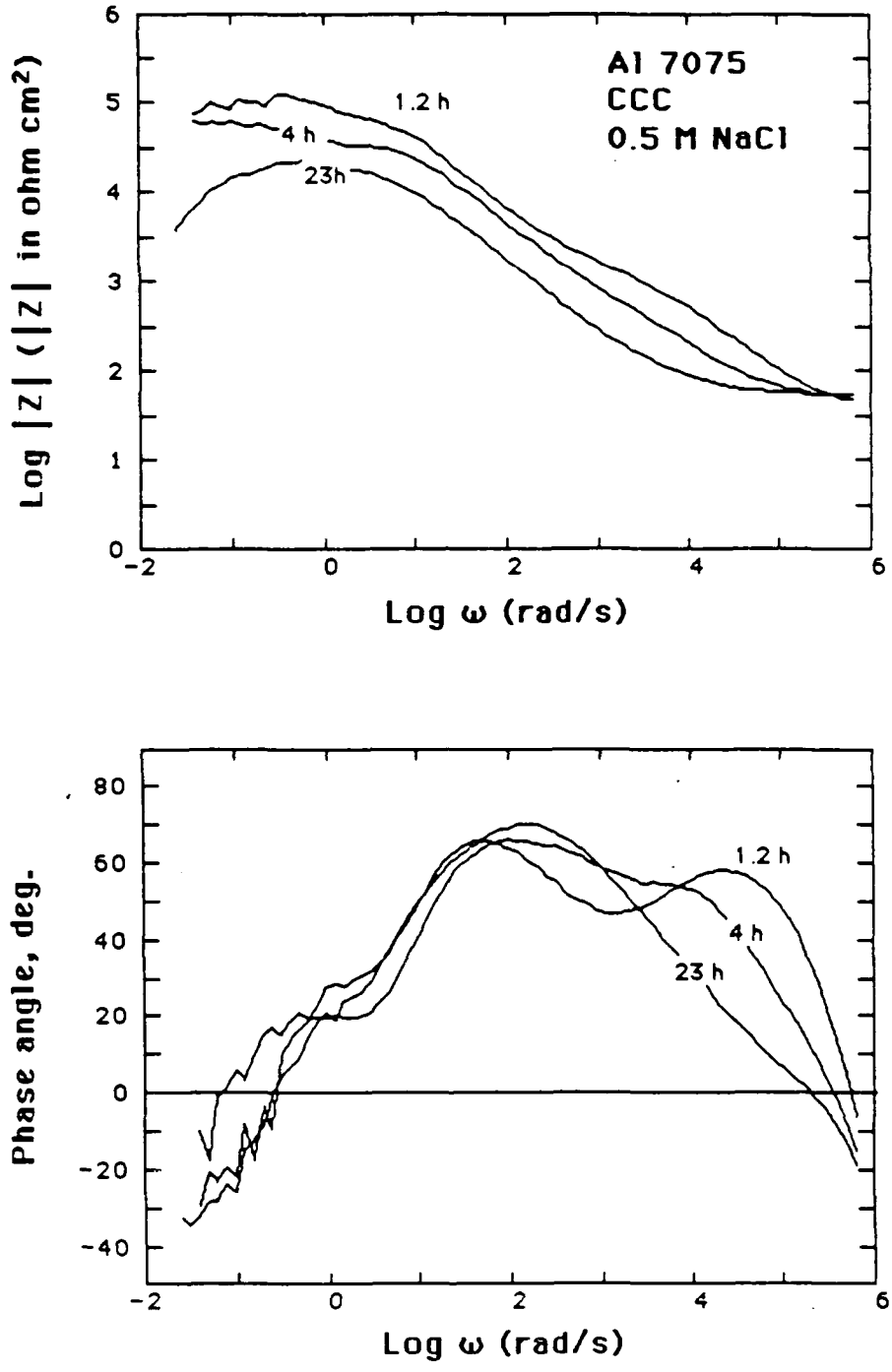

Fig. 23 Bode plots for chromate conversion coated (CCC) Al 7075-T73 in aerated 0.5 M NaCl after 1, 4 and 23 h.

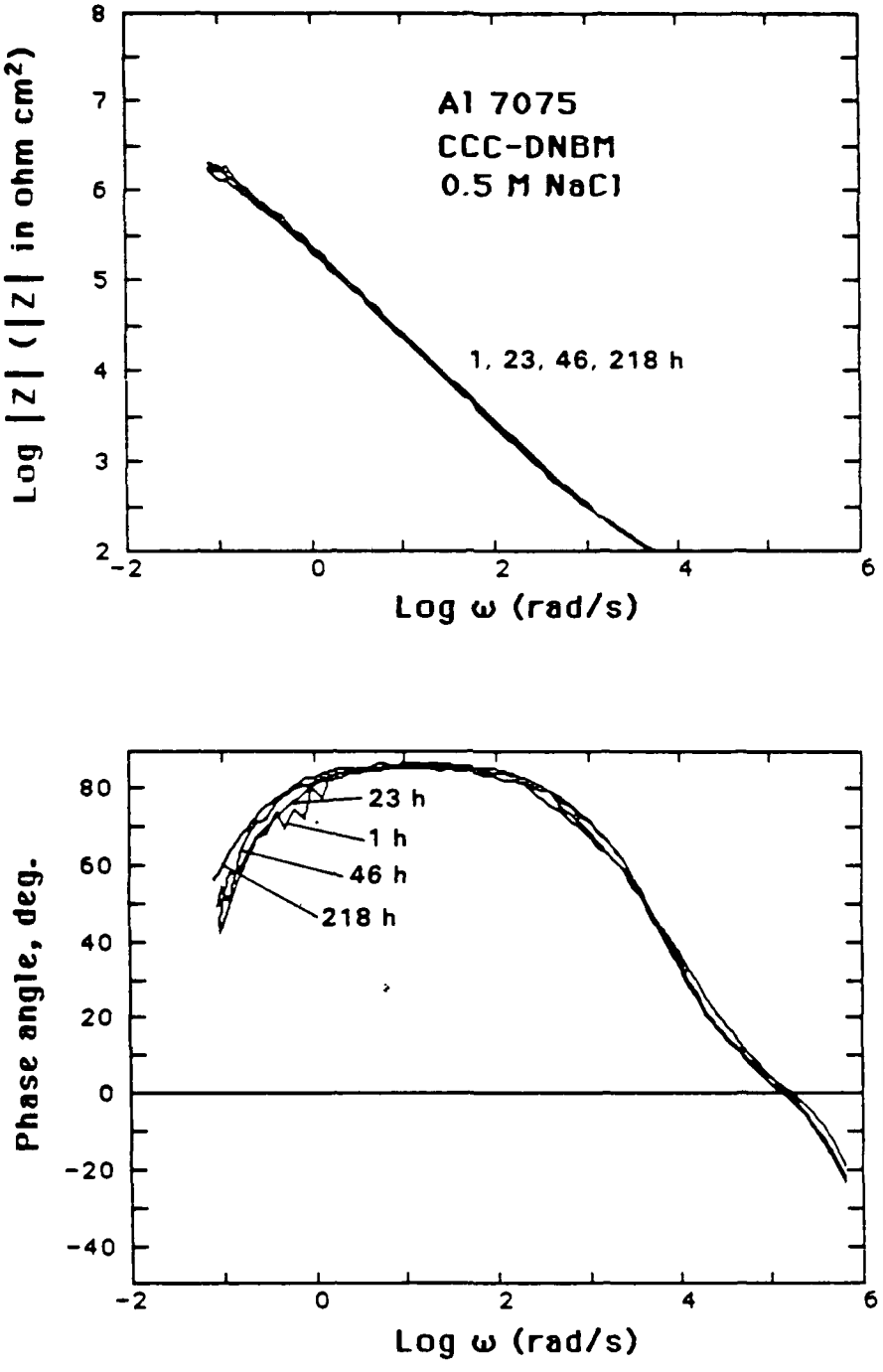

Fig. 24 Bode plots for chromate conversion coated Al 7075 treated with DNBM (CCC-DNBM) in aerated 0.5 M NaCl after 1, 23, 46 and 218 h.

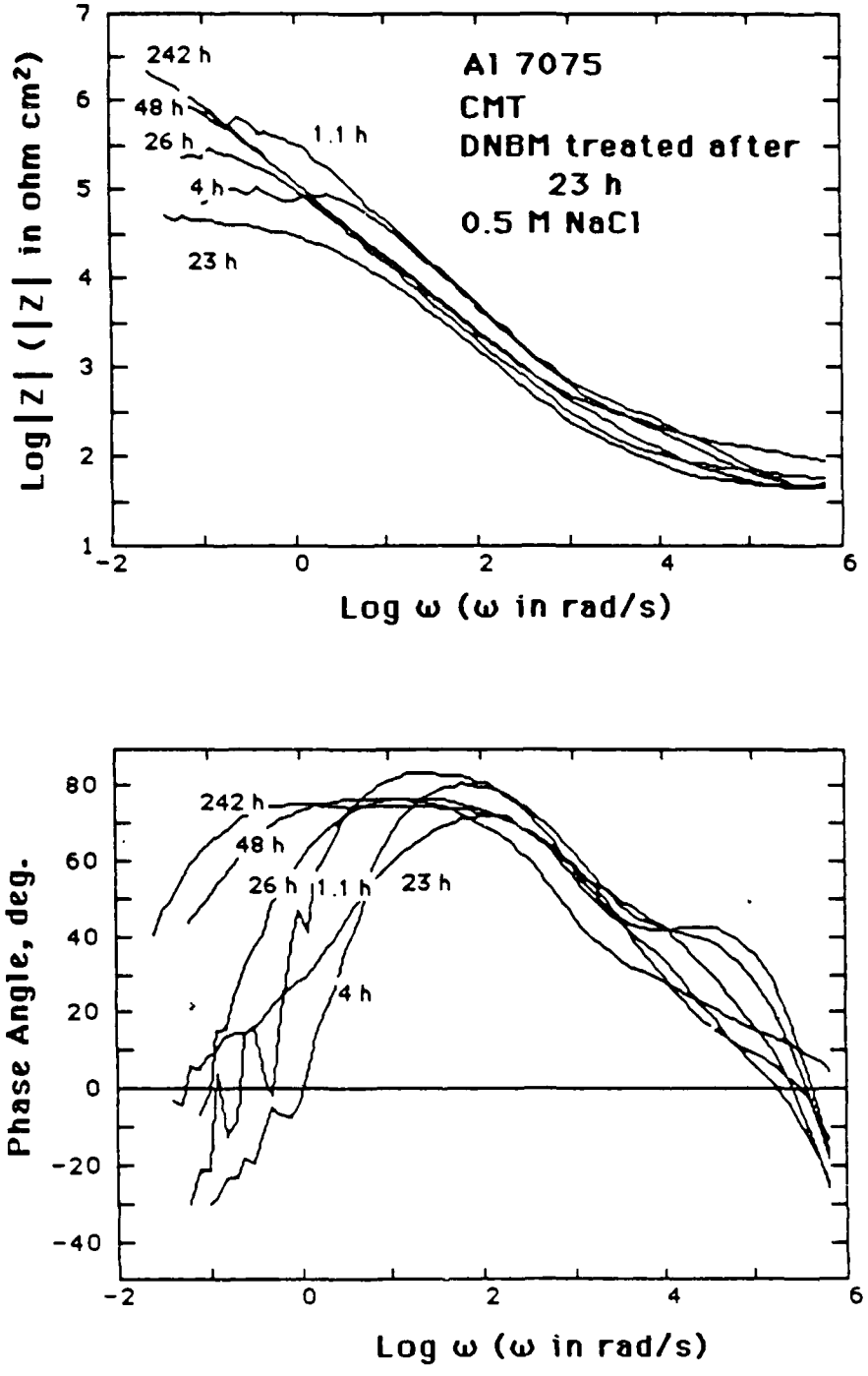

Fig. 25 Bode plots for chromate containing molybdate conversion-coated Al 7075 in aerated 0.5 M NaCl between 1 and 242 h. The surface was additionally treated with DNBM after 23 h.

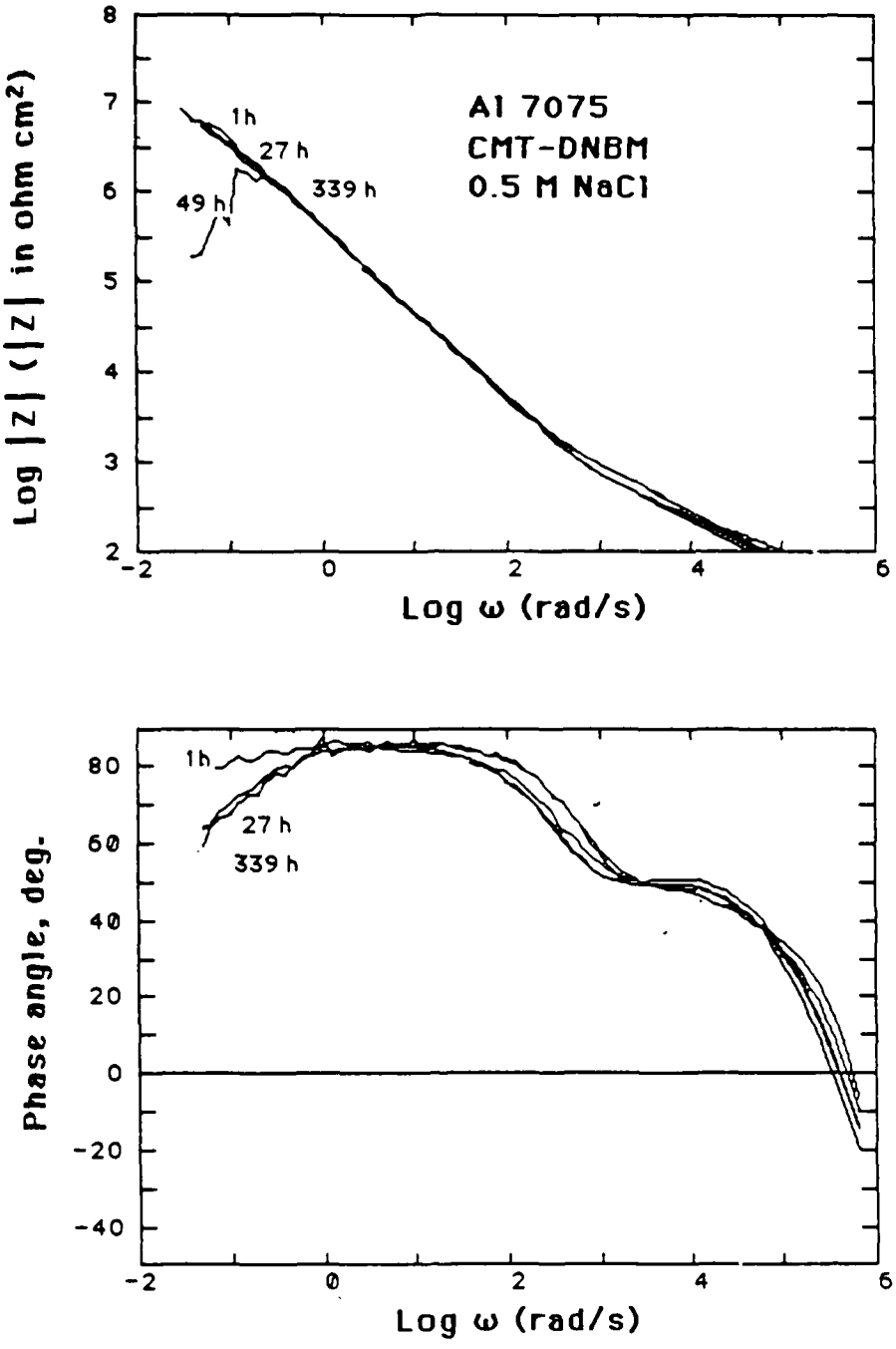

Fig. 26 Bode plots for chromate containing molybdate conversion-coated and DNBM treated Al 7075 in aerated 0.5 M NaCl between 1 and 339 h.

Figure 27 provides a summary of the impedance analysis of the Al 7075 materials. Figure 27a shows the time dependence for R_p. The conversion coatings provide an initial improvement in corrosion resistance in 0.5 M NaCl by about a factor of 5 for the CCC-treated specimen and 20 for the CMT-treated alloy over the polished untreated alloy. In time, R_p decreases and by extrapolation will compare to the untreated alloy after about 100 h immersion in the 0.5 M NaCl. For the conversion coatings treated with the DNBM, however, the corrosion resistance remains near 10^7 Ω-cm^2 for more than 2000 h, representing a 1000-fold improvement in corrosion resistance over the bare alloy, and more than a 100-fold improvement over the conversion-coated material. Note that the DNBM is an ionically conducting material which is absorbed by the porous conversion coating. Therefore, it is not anticipated that this treatment will significantly, if at all, increase the resistivity of the coating. Treatment of conversion coatings with DNBM should be considered as a possible corrosion protection method for Al alloys requiring low surface resistivity.

The capacitances of the conversion-coated alloys CCC, CMT and CMT-DNBM are all initially near 2 μF/cm^2, which suggests that the original film thicknesses are more or less comparable (Fig. 27b). The CCC-DNBM coating appears to be somewhat thinner than the others, having an initial capacitance which is near 5 μF/cm^2. The bare alloy has an initial capacitance of 20 μF/cm^2. Without DNBM, the capacitances for the coated alloys (CCC and CMT in Fig. 27b) increase, suggesting thinning of the conversion coating. The development of a high pseudo-capacitance in parallel with the coating film due to the onset of pitting offers an alternative explanation for the decreasing capacitance with time. However, the CMT specimen, which was treated with DNBM after some degradation, showed reversal of the polarization resistance to initial values, but its capacitance did not reverse back to the initial 2 μF/cm^2 (Fig. 27b). This suggests that in the initial stages, the degradation process of conversion-coated Al occurs via overall film degradation rather than high localized corrosion at defects.

The corrosion potential, E_o, for the conversion-coated specimens (Fig. 27c) offers little additional information. The potential for the bare alloy starts at a low value of -800 mV and increases to over -740 mV after 10 h. E_o, for the conversion-coated specimens, is initially between -750 and -710 mV, and remains more or less constant with time.

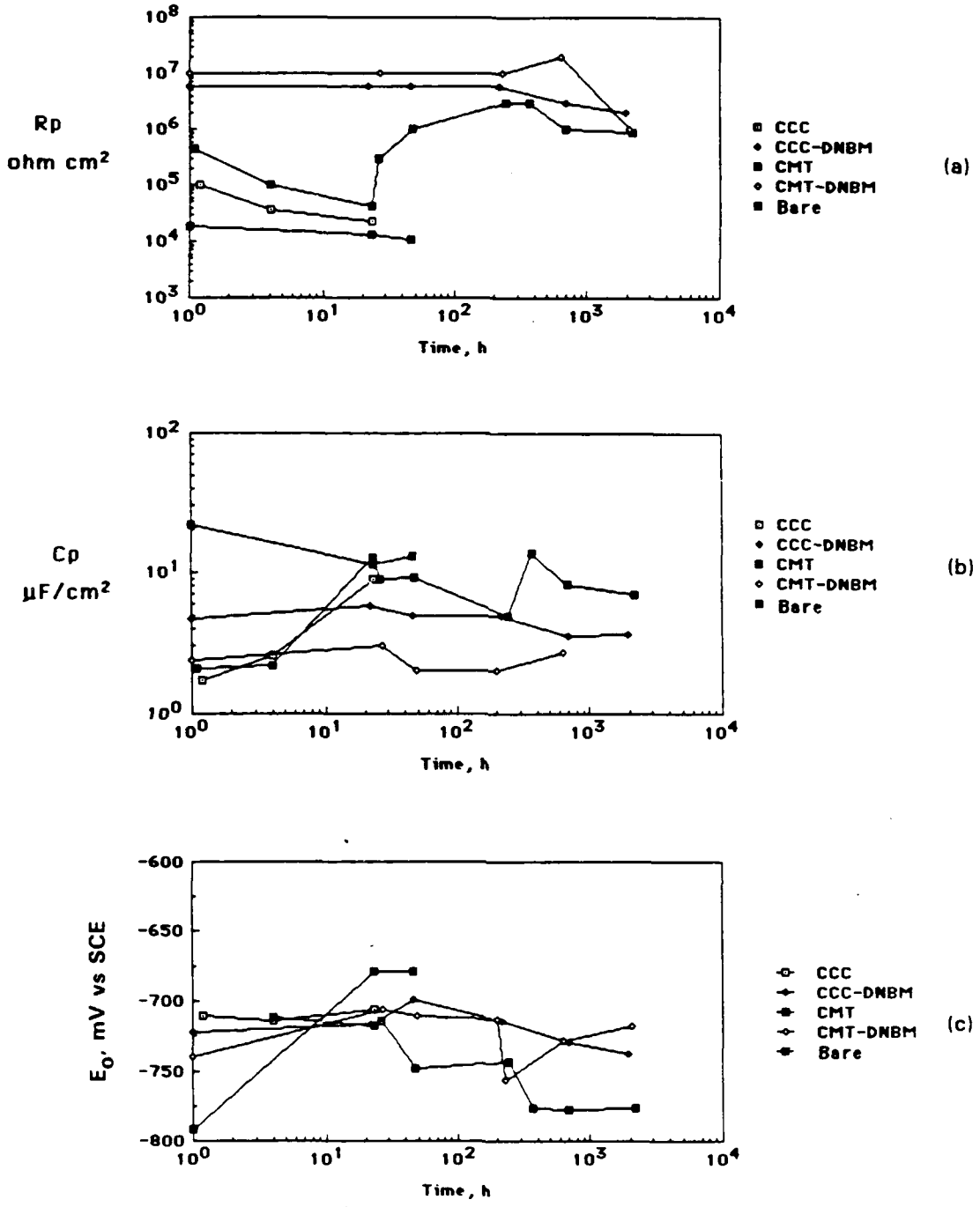

Fig. 27 Time dependence for R_p, C_p and E_o for the Al 7075 alloys having different surface treatments.

4.0 SUMMARY, CONCLUSIONS AND RECOMMENDATIONS

Three ac methods have been described in this report: (1) fatigue admittance, (2) compliance monitoring and (3) electrochemical impedance spectroscopy (EIS). The fatigue admittance method provides a measure of the coupling of electrochemical reactions to the cyclic displacement of a crack tip. This current can be measured as a function of potential to evaluate the corrosion potential of the crack tip, E_C. Compliance monitoring makes use of phase-sensitive detection of the cyclic displacement of a fatigue crack. The method is at least as sensitive as electric resistance methods for evaluation of crack growth rates to within 0.01 μm/cycle, but does not inadvertently influence crack wall electrochemical reactions with the passage of large sample currents. Electrochemical impedance methods provide a characterization of the corrosion behavior and the nature of protective films, as well as of the action of inhibitors on boldly exposed surfaces.

Fatigue admittance, whereby the fatigue current generated by cyclic displacement of the mouth of a fatigue crack is measured, provides a measure for the extent to which electrochemical processes couple to fatigue. The point where the fatigue current reaches a minimum is related to the corrosion potential of the crack tip and its anodic displacement provides a measure of the anodic activity of the crack tip. Injection of an isopropanol solution of DNBM into the crack tip of Al 7075-T73 decreases the anodic shift of the crack tip potential and the fatigue current at open circuit, and decreases the rate of anodic electrochemical reactions in the crack tip by nearly a factor of 100. The maximum load was found to have a dominant influence on the electrochemical kinetics in the crack tip during CF of Al 7075-T73 at 4 Hz. The larger the maximum stress intensity, the greater the rate of the anodic reaction at the crack tip. Injection of the isopropanol solution of DNBM into a fatigue crack in 4340 steel decreases the crack growth rate by about an order of magnitude as compared to 0.5 M NaCl and eliminates the negative shift of the corrosion potential of the crack tip.

CF of 4340 steel in near-neutral solutions is governed by hydrogen permeation. For long cracks and in the absence of inhibitors, polarization of the sample to potentials between -900 and -1000 mV continuously increases the crack growth rate. The anionic inhibitors of DNBM in bulk solution at levels of 0.01 M have a very small influence on the open-circuit CF rate of 4340 steel, as compared to their behavior when

incorporated in the organic DNBM formulation. Nevertheless, the molybdate and dichromate inhibitors decrease the rate of the anodic process in the crack tip and borate decreases the CF rate under cathodic polarization. Passivation processes appear to decrease the cathodic acceleration of CF.

EIS demonstrates that the mixed inhibitor DNBM treatment of 4340 steel diminishes the corrosion rate by nearly a factor of 10 in aerated 0.5 M NaCl. The impedance spectra and the independence of the corrosion potential on rotation show that the mechanism of inhibition involves the formation of a three-dimensional interphase at the metal surface, which blocks the oxygen reduction reaction.

Impedance spectra obtained for conversion-coatings containing various inhibiting species show that conventional CCCs on Al 7075 have a protective life of about 100 h when continuously immersed in aerated 0.5 M NaCl. Conversion coatings containing Mo compounds, as compared to the conventional conversion coating, improve the initial corrosion resistance of typically conversion-coated Al 7075 immersed in neutral 0.5 M NaCl by a factor of 4. In general, conversion coatings containing absorbed DNBM in xylene show a 100-fold increase in corrosion resistance over the coatings not having any DNBM. The coatings with absorbed DNBM inhibitor in an organic phase do not degrade significantly for over 1000 h immersion in 0.5 M NaCl. It is recommended that additional testing of conversion coatings on Al alloys containing absorbed organic phase inhibitors be performed under a variety of conditions so that these alloys may ultimately be qualified for use on aerospace structures. DNBM inhibited conversion coatings probably have an additional advantage in that they do not increase the electrical resistance of the coating.

5.0 REFERENCES

1. R. Parkins, Metal Sci. 13 (7), 381 (1979).

2. R. Parkins and B.S. Greenwell, Metal Sci. 11, 406 (1977).

3. M. Kendig and F. Mansfeld, "Application of Electrochemical and Mechanical Impedance Techniques for Evaluation of SCC and CF," Paper No. 190, NACE, Corrosion/86 (1986).

4. V.S. Agarwala, D.A. Berman and G. Kohlhass, "Causes and Prevention of Structural Materials Failure in Naval Environments," Paper No. 115, NACE, Corrosion/84, New Orleans, LA (1984).

5. D.E. Talbot, J.W. Martin, C. Chandler and M.I. Sanderson, Metal Techn. 9, 130 (1980).

6. T. Pyle, V. Rollins and D. Howard, J. Electrochem Soc. 112, 1445 (1975).

7. A. Roelandt and J. Vereecken, Surface Technology 9, 347 (1979).

8. G.C. Ford, Brit. Corr. J. 17, 13 (1982).

9. L.E. Eiselstein, M.C.H. McKubre and R.D. Caligiuri, "Prediction of Crack Growth in Aqueous Environments," N00014-82-K-0343, (1983).

10. V. Agarwala and J.J. DeLuccia, "Modification of Crack Tip Chemistry Inhibitors for Corrosion and SCC of High Strength Alloys," in Embrittlement by Localized Crack Environments, R. Gaigloff, ed., p. 405, AIME (1980).

11. V. Agarwala, New Materials and New Processes 3, 178 (1985).

12. V. Agarwala, "Crack Arrestment Compounds of Corrosion Fatigue for High Strength Steel," Report No. NADC-802290-60, Jan. 1981.

13. M.W. Kendig, A.T. Allen and F. Mansfeld, J. Electrochem. Soc. 131, 935 (1984).

14. V. Agarwala, personal communication.

15. J. Scully and P. Moran, J. Electrochem. Soc., to be published.

16. F. Mansfeld, Corrosion 37, 301 (1981).

17. F. Mansfeld, M.W. Kendig and S. Tsai, Corrosion 38, 556 (1982).

18. W.J. Lorenz and F. Mansfeld, Corr. Sci. 21, 647 (1981).

19. F. Mansfeld and M.W. Kendig, Werkstoffe und Korrosion 34, 397 (1983).

20. F. Mansfeld, M.W. Kendig and W.J. Lorenz, J. Electrochem. Soc. 132, 290 (1985).

21. F. Mansfeld, M.W. Kendig and S.Tsai, Corrosion 38, 478 (1982).

22. M.W. Kendig, F. Mansfeld and S. Tsai, Corr. Sci. 23, 317 (1983).

23. F. Mansfeld and M.W. Kendig, ASTM STP 866, 122 (1985).

24. F. Mansfeld and M.W. Kendig, Werkstoffe und Korrosion 36, 473 (1985).

25. F. Mansfeld and M.W. Kendig, Corrosion 41, 490 (1985).

26. W.J. Lorenz and F. Mansfeld, Electrochem. Acta. 31, 467 (1986).

27. F. Mansfeld and S.L. Jeanjaquet, "Evaluation of Corrosion Protection Measures for Metal Matrix Composites," Corr. Sci. 26(9), 727 (1987).

28. K. Fertig, Rockwell Science Center, Palo Alto Laboratory, Palo Alto, CA, personal communication, 1987.

29. F. Mansfeld, Dept. of Metallurgy and Materials Science, University of Southern California, Los Angeles, CA, personal communication, 1987.

6.0 ACKNOWLEDGEMENT

The authors gratefully acknowledge direct collaboration in part of this project and useful discussions with Dr. Vinod S. Agarwala of the Naval Air Development Center.

APPENDIX I. SYMBOLS AND ABBREVIATIONS

I_{ac} = Fatigue current which is the ac current having the same frequency as the applied cyclic load

I_{dc} = Polarization current

E_o = Open circuit or corrosion potential

E_c = Corrosion potential of the crack tip

ΔE = $E_c - E_o$

dA/dN_o = Crack growth rate at E_o

dA/dN_c = Crack growth rate below -900 mV vs SCE

Cathodic accleration = $dA/dN_c - dA/dN_o$

ω = Angular frequency in rad/s

f = Frequency in Hz

Z = Complex impedance in $\Omega\text{-cm}^2$

CF = Corrosion fatigue

SCC = Stress corrosion cracking

R_{xp} = Observed polarization resistance taken as $\left(\frac{dE}{dI}\right)_{I_2 = 0}$

R_p = Specific polarization resistance in units of $\Omega\text{-cm}^2$

C_p = Specific capacitance in units of $\mu F/cm^2$

$I_{ac}(E_o)$ = I_{ac} at E_o

$I_{ac}(E_c)$ = I_{ac} at E_c

SCE = Saturated calomel electrode

ΔK_{si} = Stress intensity

RCE = Rotating cylindrical electrode

LIA = Lock-in amplifier

EIS = Electrochemical impedance spectroscopy

CCC	=	Chromate conversion coated
CMT	=	Conversion coating containing molybdate
DNBM	=	Dichromate, nitrite, borate and molybdate

APPENDIX II. STATISTICAL ANALYSIS

Let y_{ijkl} be the ijkl'th observation in an experiment with the four variables whose settings are specified by i,j,k and l, respectively (e.g., for the case that each variable has just two levels, i takes on the values 1 and 2). Let i = 1,...,I, j = 1,...,J, etc.

Let $y_{ijk.}$ represent the average of the y_{ijkl} over l. More generally, the dot notation is used to mean average over the deleted subscripts. Thus,

$$y_{.j.l} = (1/IK) \sum_i \sum_k y_{ijkl}$$

We take as our model

$$y_{ijklv} = \mu + \alpha^{A}_{i} + \alpha^{B}_{j} + \alpha^{C}_{j} + \alpha^{D}_{l} + \alpha^{AB}_{ij} + \alpha^{AC}_{ik} +$$

$$\ldots + \alpha^{ABC}_{ijk} + \ldots + \alpha^{BCD}_{jkl} + \alpha^{ABCD}_{ijkl} + \epsilon_{ijklv}$$

Each of the "effects", e.g., α^{ABC}_{ijk}, sum to zero for each of their subscripts. That is,

$$\alpha^{ABC}_{.jk} = \alpha^{ABC}_{i.k} = \alpha^{ABC}_{ij.} = 0$$

An effect is estimated by the following pattern:

$$\alpha^{A}_{i} = y_{i....} - y_{.....}$$

$$\alpha^{AB}_{ij} = y_{ij...} - y_{i...} - y_{.j...} + y_{...}$$

$$\alpha^{ABC}_{ijk} = y_{ijk..} - y_{ij...} - y_{i.k..} - y_{.jk..} + y_{i....} + y_{.j...}$$

$$+ y_{..k..} - y_{.....},$$

etc.

The analysis of variance table takes the following form:

Source	Sum of Squares	Degrees of Freedom	Estimate of MS
A Main Effects	$SS_A = JKLM \Sigma (a^A{}_i)^2$	I-1	$\sigma^2 + JKLM\sigma^2_A$
B Main Effects	$SS_A = IKLM \Sigma (a^B{}_i)^2$	J-1	$\sigma^2 + IKLM\sigma^2_B$
AB Interactions	$SS_{AB} = KLM \Sigma\Sigma (a^{AB}{}_{ij})^2$	(I-1)(J-1)	$\sigma^2 + KLM\sigma^2_{AB}$
ABC Interactions	$SS_{ABC} = LM \Sigma\Sigma\Sigma (a^{ABC}{}_{ijk})^2$	(I-1)(J-1)(K-1)	$\sigma^2 + LM\sigma^2_{ABC}$
ABCD Interactions	$SS_{ABCD} = \Sigma\Sigma\Sigma\Sigma (a^{ABCD}{}_{ijkl})^2$	(I-1)(J-1)(K-1)(L-1)	$\sigma^2 + \sigma^2_{ABCD}$
Error	$SS_e = \Sigma\Sigma\Sigma\Sigma\Sigma (y_{ijklm} - y....)^2$	IJKL(M-1)	σ^2

In the above,

$$\sigma^2_A = \Sigma (\alpha^A{}_i)^2/(I-1), \text{ etc.}$$

Thus, to say effect A is zero (all $\alpha^A{}_i = 0$) is equivalent to saying $\sigma^2_A = 0$.

The mean square, MS, is defined as the sum of squares, SS, divided by the associated degrees of freedom. For two levels, I=J=K=L=2, M=1 (no replication). Therefore, for a full interaction model, there are no degrees of freedom left over for error. In such cases, it is traditional to assume that the higher order interactions are zero. Thus, if it is assumed the ABCD interaction is zero ($\sigma^{2ABCD} = 0$), then the associated MS can be used to estimate the error. For two levels, it will have one degree of freedom ((I-1)(J-1)(K-1)(L-1) = 1)). It can be used in all the F-tests to determine if any effects are significant. In general, compute

$$F(N_i, N_{error}) = \text{MS for effect i/MS for error.}$$

N_i is the degrees of freedom for the effect i and N_{error} is the degrees of freedom for the error. For two levels, these will be 1 and 1, respectively.

Note that under the hypothesis that the effect is zero, the computed F will be distributed according to the F-distribution, with N_i and N_{error} degrees of freedom. Look at the above table and see, for example, that (when $\sigma^{2ABCD} = 0$) under the hypothesis that $\sigma^{2A} = 0$, we have $E(MS_A) = \sigma^2$ and $E(MS_{ABCD}) = \sigma^2$. Thus, the numerator and

denominator for F(1,1) for effect A have the same expectation. Orthogonality of the design implies that they are independent. Under normality of errors assumption, they will be chi-squares. Thus, under the hypothesis that $\sigma^{2A} = 0$, we have that F(1,1) for effect A is really an F-variate with 1 and 1 degrees of freedom.

The above calculations are trivial for a factorial design. In general, we can fill in a table of "effect" signs that are a direct function of the levels of a variable. Put in a +1 when the variable is high, put in a -1 otherwise. For interactions between variables, use ++=+, +-=-, -+=- and —=+. A table for three variables looks like:

Run No.	1	2	3	4	5	6	7	8
Treatment	000	100	010	001	110	101	011	111
Effects								
M	+	+	+	+	+	+	+	+
A	-	+	-	-	+	+	-	+
B	-	-	+	-	+	-	+	+
C	-	-	-	+	-	+	+	+
AB	+	-	-	+	+	-	-	+
BC	+	+	-	-	-	-	+	+
AC	+	-	+	-	-	+	-	+
ABC	-	+	+	+	-	-	-	+

Thus, the signs for the AB interaction row are the signs you get by multiplying the signs in the A row by the signs in the B row. The signs in the ABC row are obtained by A times BC or B times AC, etc. Note that all rows are orthogonal to each other.

The divisor in a 2^k factorial design is 2^k. In the above example, this will be 8. In your experiment, it will be 16. To estimate the MS for an effect, use the above table of signs to combine the runs and divide by the divisor. Thus, the MS effect for AC interaction is

$$\text{MS for AC} = (R1 + R3 + R6 + R8 - R2 - R4 - R5 - R7)^2/8$$

This is algebraically equivalent to

$$SS_{AC} = J \sum\sum (a^{AC}_{ik})^2/[(I-1)(K-1)] \text{ when } I=K=2.$$

DISTRIBUTION LIST (Continued)

	No of Copies
Dr. H. Leidheiser, Jr. Center for Coatings and Surface Research Lehigh University, Bethlehem, PA 18015	1
Dr. M. Kendig Rockwell International Science Center 1049 Camino Dos Rios, P.O. Box 1085 Thousand Oaks, CA 91360	1
Dr. C. McMahon, LRSM University of Pennsylvania Philadelphia, PA 19104	1
Defense Technical Information Center Attn: DTIC-DDA-1, Cameron Station Bldg. 5 Alexandria, VA 22314	12
NAVAIRDEVCEN (3 for Code 8131) (50 for Code 6062 - V. Agarwala)	53

DISTRIBUTION LIST (Continued)

	No. of Copies
Office of Naval Technology NAVMAT-0725 800 N. Quincy Street, Arlington, VA 22217 (Mr. J. J. Kelly)	1
Naval Research Laboratory 4555 Overlook Ave., Washington, DC 20375 (Dr. B. Rath)	1
David Taylor Ship Research Development Center Code (281), Annapolis, MD 21402 (Mr. A. G. S. Morton, Mr. G. Wacker)	2
Naval Surface Weapons Center (Code R-30) White Oak, Silver Spring, MD 20910	1
Naval Air Propulsion Center (Code PE-72) Trenton, NJ 08628 (Mr. A. J. Dorazio)	1
Naval Underwater Systems Center (Code 4493) New London, CT 06320 (Dr. R. G. Kasper)	1
AFOSR, Bolling AFB Washington, DC 20332 (Dr. A. Rosenstein)	1
Wright-Patterson AFB WPAFB (AFWAL MLSA), OH 45433 (Mr. B. Cohen)	1
Air Force Logistics Center (MMEMC) Warner-Robbins AFB, Warner, GA 31098 (Mr. W. Thompson)	1
Army Research Office P.O Box 12211, Research Triangle Park, NC 27709 (Dr. R. Reeber)	1
U.S. Army Materials and Mechanics Research Center (DRXMR-EM), Watertown, MA 02172 (Dr. M. Levy)	1
U.S. Army Armament R & D Command (DRDAR-SCM) Bldg. 355, Dover, NJ 07801	1
U.S. Army Mobility Equipment R & D Command (DRDME-VC) Fort Belvoir, VA 22060 (Mr. D. A. Emeric)	1
National Bureau of Standards Washington, DC 20234	1

DISTRIBUTION LIST

REPORT NO. NADC-87183-60

	No. of Copies
Naval Air Systems Command (2 for AIR-7226) (1 for AIR-31A) (2 for AIR-5304) (1 for AIR-5142) (1 for AIR-03D)	6
Commanding Officer Naval Air Rework Facility, Attn: Code (340) Naval Air Station, Alameda, CA 94501	1
Commanding Officer Naval Air Rework Facility, Attn: Code (340) Naval Air Station, Jacksonville, FL 32212	1
Commanding Officer Naval Air Rework Facility, Attn: Code (340) Naval Air Station, Norfolk, VA 23511	1
Commanding Officer Naval Air Rework Facility, Attn: Code (340) Naval Air Station, North Island San Diego, CA 92135	1
Commanding Officer Naval Air Rework Facility, Attn: Code (340) Naval Air Station, Pensacole, Fl 32508	1
Commanding Officer Naval Air Rework Facility, Attn: Code (340) Marine Corp. Air Station, Cherry Point, NC 28533	1
Commanding Officer Naval Air Force, U.S. Atlantic Fleet Attn: Code 5281, Norfolk, VA 23511	1
Commander Naval Air Force, U.S. Pacific Fleet Attn: Code 7412, San Diego, CA 92135	1
Naval Sea Systems Command Washington, DC 20362	1
Office of Chief of Naval Research 800 N. Quincy Street Arlington, VA 2217-5000 (Dr. A. D. Wood, Code OOPA)	1
Office of Naval Research 800 N. Quincy Street, Arlington, VA 22217 (Dr. A. J. Sedriks)	1

END

DATE

FILMED

5-88

DTIC